ACS APPLIED ENERGY MATERIALS

Article

Surface Sensitive Nickel Electrodeposition in Deep Eutectic Solvent

Paula Sebastian, Marina Inés I. Giannotti, Elvira Gómez, and Juan M. Feliu

ACS Appl. Energy Mater., **Just Accepted Manuscript** • DOI: 10.1021/acsaem.7b00177 • Publication Date (Web): 16 Feb 2018

ACS Publications

ACS Applied Energy Materials is published by the American Chemical Society. 1155 Sixteenth Street N.W., Washington, DC 20036

Surface Sensitive Nickel Electrodeposition in Deep Eutectic Solvent.

P. Sebastian[†], M. I. Giannotti[‡,§,∥], E. Gómez[∥] J. M. Feliu[†*]*

† Institute of Electrochemistry, University of Alicante, Apartado, 99, 03080 Alicante, Spain.

‡ Centro de Investigación Biomédica en Red (CIBER), Instituto de Salud Carlos III, Monforte de Lemos, 3-5, 28029 Madrid, Spain.

§ Institute for Bioengineering of Catalonia (IBEC), Baldiri Reixac, 15-21, 08028 Barcelona, Spain.

∥ Department de Ciencia dels Materials i Química Física, University of Barcelona, Martí i Franquès, 1, 08028 Barcelona, Spain.

Corresponding Author
*E-mail: e.gomez@ub.edu
*E-mail: j.feliu@ua.es

KEYWORDS

Deep eutectic solvent, nickel electrodeposition, glassy carbon, platinum electrode, Pt(111), SEM, AFM, nanostructures, surface sensitive.

ABSTRACT

The first steps of nickel electrodeposition in a deep eutectic solvent (DES) are analysed in detail. Several substrates from glassy carbon to Pt(111) were investigated pointing out the surface sensitivity of the nucleation and growth mechanism. For that, cyclic voltammetry and chronoamperometry, in combination with scanning electron microscopy (SEM), were employed. X-ray diffraction (XRD) and atomic force microscopy (AFM) were used to more deeply analyse the Ni deposition on Pt substrates.

In a 0.1 M $NiCl_2$ + DES solution (at 70ºC), the nickel deposition on glassy carbon takes place within the potential limits of the electrode in the blank solution. Although, the electrochemical window of Pt|DES is considerably shorter than on glassy carbon|DES, it was still sufficient for the nickel deposition. On Pt electrode, the negative potential limit was enlarged while the nickel deposit growed, likely because of the lower catalytic activity of the nickel towards the reduction of the DES. At lower overpotentials, different hydrogenated Ni structures were favoured, most likely because of the DES co-

reduction on the Pt substrate. Nanometric metallic nickel grains of rounded shape were obtained in any substrate, as evidenced by the FE-SEM. Passivation phenomena, related to the formation of Ni oxide and Ni hydroxylated species, were observed at high applied overpotentials. At low deposited charge, on Pt(111) the AFM measurements showed the formation of rounded nanometric particles of Ni, which rearranged and formed small triangular arrays at sufficiently low applied overpotential (Scheme 1). This particle pattern was induced by the <111> orientation and related to surface sensitivity of the nickel deposition in DES. The present work provides deep insights into the Ni electrodeposition mechanism in the selected deep eutectic solvent.

Scheme 1. Representation of the Ni(II) electrodeposition in DES on Pt(111) and AFM image (2 x 2 μm^2) of the Ni clusters.

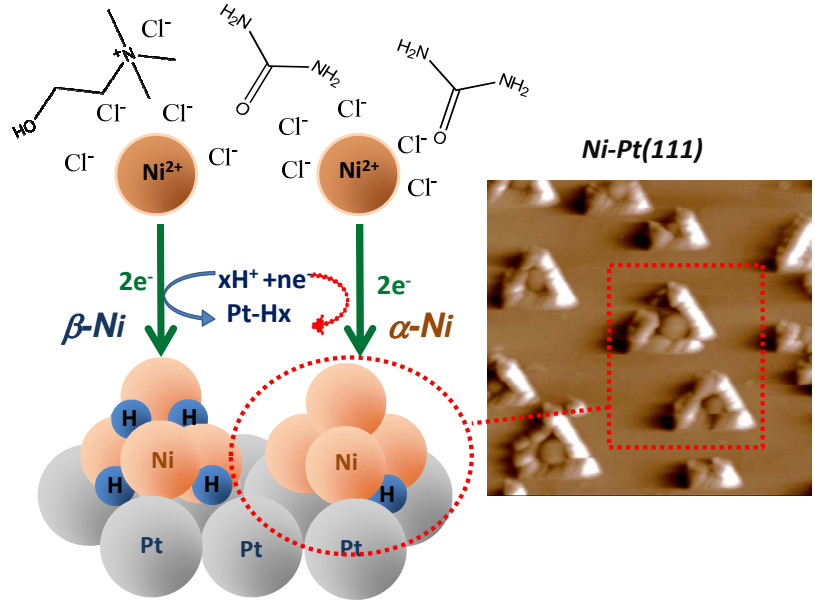

INTRODUCTION

Nickel has been extensively used for coatings to prevent the corrosion of the materials.[1] Moreover, and because of their magnetic properties, several Ni-alloys containing mainly Fe, Co or W have been investigated and progressively incorporated in electronic devices such as sensors or devices for memory storage.[2-9] Besides the interest of nickel in the electronics, nickel was also proved to be a good candidate in the design of new catalysts. So, the combination of nickel with other metals like gold or platinum improves the catalytic activity in several reactions of interest. For instance, nickel supported on gold electrode improves the oxidation of organic compounds in alkaline media, this includes glucose, thus being a potential biosensor.[10] On the other hand, the presence of Ni on gold also decreases the overpotential required for the oxygen evolution reaction (OER) due to the surface activation by the formation of hydroxylated nickel species NiO_xH_y.[11-13] Platinum modified by small amounts of NiO_xH_y has been demonstrated to considerably improve the hydrogen reduction reaction (HER) in alkaline media[14-19] while Ni-Pt-Ni alloys are better catalyst for the oxygen reduction reaction (ORR) in comparison with bare platinum.[20, 21] All these reactions (ORR, HER and OER) are of paramount importance for the design of more efficient fuel cells. In other fields, different routes to synthetize nanowires containing nickel and gold have recently been investigated for drug delivery compounds and medical applications.[22]

Definitely, nickel is truly desirable in a broad field of applications. In addition, its relative low cost and abundance motivates their use and incorporation in new devices. Finding new sustainable routes that allow modifying surfaces with nickel providing new properties becomes then very demanded.

One optimal way to obtain nickel alloys or nickel coatings is by using classical electrochemical techniques, i.e. by metal electrodeposition. This methodology is simple since it uses a low amount of energy allowing the metal electrodeposition at room temperature. By controlling parameters such as applied current density/potential or bath composition it is possible to modulate the electrodeposition process.[23] However, aqueous electrolytes show some drawbacks for the nickel electrodeposition. The most important inconvenient is that the nickel deposition usually overlaps with the reduction of the solvent because of the nickel overpotential towards the hydrogen evolution, in combination with the high overpotential required to reduce the metal. The overlapping with the solvent reduction could promote the formation of hydroxylated species and the increase of the porosity of the coatings due to the hydrogen bubbles formation.[1, 24] To deal with these inconveniences, rigorous control of the pH and several additives, some of them hazardous, are required in aqueous solution.

One alternative to the use of traditional aqueous baths are Room Temperature Ionic Liquids (RTILs). Since RTILs have a wide electrochemical window (3-5 V) and sufficient conductivity, these new solvents are suitable for metal electrodeposition applications, although they show relatively low metal solubility.[25-34] Unfortunately, the high cost of RTILs limits bulk applications and more feasible alternatives are explored. In this context, Deep Eutectic Solvents (DESs) have emerged as the cheaper and greener alternative to RTILs.[35-37] DES share many benefits with RTILs: tuneability, enough

conductivity, similar mass transport properties and a widerer electrochemical window than aqueous electrolytes. In addition, they show better metal solubility than RTILs. However, unlike RTILs, DESs are less chemically and thermally stable, as evidenced by their shorter electrochemical window that decreases slightly with the increase of the temperature. DESs have been employed for metal electrodeposition, showing that they allow modulating the deposition process. In the case of nickel, different structures were found depending on both the DES composition and substrates employed.[38-47] Recently, Ustarroz et al. investigated the nickel deposition on glassy carbon using a ChCl/urea based DES and described that nickel deposition involved the formation of nanostructures.[48]

Here, we investigated in detail the electrodeposition of nickel in a DES based on the mixture ChCl/urea. For that, two substrates of different nature were chosen: glassy carbon and platinum. More specifically, a platinum bead electrode was firstly employed and afterwards a Pt(111) single crystal electrode was used to investigate the possible surface sensitivity of the nickel deposition. The final purpose of comparing these two dissimilar substrates is evaluating the availability of this DES to modify a platinum electrode, which is considerably more catalytic than glassy carbon, and also how both the media and specific orientation of the surface influences the nickel deposition.

To investigate nickel electrodeposition, cyclic voltammetry and chronoamperometry were used. The chronoamperometric data were analysed under the light of the classical nucleation and growth mechanism. The morphology of the nickel deposits was analysed by using Field Emission Scanning Electron microscopy (FE-SEM), at first on glassy carbon and later on the different Pt electrodes. Finally, atomic force microscopy (AFM) was employed to analyse a Pt(111) surface modified by low amounts of nickel, in order

to assess the influence of the specific surface orientation on the initial steps of Ni electrodeposition in DES.

EXPERIMENTAL SECTION

Both choline chloride (ChCl) and urea were purchased from Merck at the highest purity available (99%). The DES was prepared by mixing stoichiometric amounts of both salts at a temperature close to 50 ^{o}C until liquid state. The molar rate between both salts in the eutectic mix is 1:2 ChCl:urea. The liquid was dried under vacuum, stirring and heating conditions (T < 50 ^{o}C) overnight. To prepare the nickel bath, a $NiCl_2{*}6H_2O$ salt of 99% purity grade purchased from Merck was dried to dehydration and added to the DES. In order to dissolve the nickel salt in the DES, the mixture was stirred, kept under vacuum and heating conditions during 24 h. The water content in DES did not overcome 1 % (Figure S1).

The employed working electrodes were a glassy carbon rod (0.0314 cm^2), a Pt polyoriented bead electrode, Pt(poly) (0.22 cm^2) and a Pt(111) single crystal (0.048 cm^2) cut from a single crystal bead following Clavilier's methodology.[49] Specific pre-treatments were used for each one of the surfaces. The glassy carbon electrode was polished to mirror finish with alumina of different grades (3.75 and 1.87 μm from VWR Prolabo), cleaned ultrasonically for 2 min in high-quality water (resistivity of 18.2 MΩ cm, MilliQ system, Millipore) and dried with argon prior to the immersion in the solution. On the other hand, both the Pt bead and the Pt(111) were cleaned by flame-annealing and cooling down under the argon atmosphere in the electrochemical cell, in order to avoid the oxygen reaction on the surface. Then the electrodes were immersed in

the DES after cooling the electrode down. In the case of Pt(111), meniscus configuration was employed.

To perform the electrochemical experiments, a thermostated cell with a three electrode configuration was employed. The reference electrode was an Ag|AgCl|Cl^- mounted in a Lugging capillary containing the DES solvent.[50] The counter electrode was a platinum spiral. The temperature was kept at 70 ^oC.

All electrochemical measurements were carried out using a potentiostat AUTOLAB PGSTAT 12 electrochemical system. The morphology of the samples was analysed using a scanning electron microscope Field Emission JSM-7100F Analytical Microscopy. X-ray photoelectron spectroscopy (XPS) measures were carried out with an K-ALPHA, Thermo Scientific. All spectra were collected using Al-K_ radiation (1486.6 eV). X-ray diffraction (XRD) patterns were recorded using a PANalytical X'Pert-PRO MRD diffractometer with parallel optical geometry in grazing incidence configuration (1º) using Cu Kα radiation (λ = 0.1542 nm). A 2θ scan, between 10 and 100º was used, with a step size of 0.05 and a measuring time of 15 s per step. AFM images were obtained with an MFP-3D atomic force microscope (Oxford Instruments Asylum Research, Santa Barbara, CA) using V-shaped Si_3N_4 cantilevers with sharp silicon tips, and having a nominal spring constant of 0.06 N m^{-1} (SNL, Bruker AFM Probes). Images were acquired in contact mode at room temperature in air or under liquid environment (ultrapure MilliQ water), and processed with the AR software. Prior to characterization the samples were exhaustively cleaned under warm water during the necessary time to remove the residues of DES.

RESULTS AND DISCUSSION

Nickel electrodeposition on glassy carbon

At first, nickel electrodeposition on glassy carbon was analysed using the solution containing 0.1 M $NiCl_2$ in DES at 70 ºC. Figure 1A shows the cyclic voltammogram of the nickel deposition on glassy carbon (black solid line) while the dashed line corresponds to the glassy carbon | DES blank solution, i.e., without the precursor. Nickel deposition starts around -1.0 V and reaches a peak current at -1.20 V (Figure 1A peak (a)). Then the current decays followed by the reduction of the solvent. In the reverse scan, the main oxidation peak appears at -0.09 V (peak (b)). Previous to this oxidation peak one small feature appears around -0.40 V (peak (p)). Both peaks are related with the oxidation/dissolution of the deposited nickel. If the negative going scan is reversed at less negative potential limit (i.e. at -1.17 V) the cyclic voltammetry draws a current loop (Figure 1A, red line), pointing out that the nickel deposition proceeds through a nucleation and growth mechanism. The preliminary voltammetric analysis shows that, under these conditions, the nickel deposition on glassy carbon takes place within the DES potential window, but the process is quite irreversible and high overpotential value is necessary to achieve the nickel deposition in DES, similar to what happens in aqueous solutions.[51] It is interesting to note that the electrochemical window is considerably narrowed when the nickel is deposited on the glassy carbon electrode, thus evidencing that the nickel deposit is more catalytic towards the solvent reduction than the glassy carbon substrate. Similar behaviour was reported by Ustarroz et al.[48] in

the same DES, but using significantly lower nickel salt concentration, conditions at which the nickel deposition almost overlaps with the onset of the solvent reduction.

Figure 1B shows several cyclic voltammograms recorded at different cathodic potential limits. Shortening enough the negative limit, the feature labelled as peak (p) was supressed in the positive scan. The relation between the charges involved within the overall oxidation and reduction voltammetric areas, (Q_{ox}/Q_{red}), decreases by sufficiently enlarging the cathodic potential limit (Table S1). Both the decrease of the Q_{ox}/Q_{red} and the appearance of the peak (p) with the enlarging of the negative potential limit could be related with surface changes due to the solvent co-reduction. Ustarroz et al. reported that the nickel deposition on glassy carbon involved the formation of hydroxylated species at the high applied overpotential.[48] So, if the reduction of the solvent involves hydrogen evolution, which is expected due to the hydrogen bond donor character of the DES, a local pH change would promote the formation of these hydroxylated species.[52] In addition, the authors reported that the formation of these hydroxylated species was supported by the progressive surface passivation as high overpotentials were applied. Here, to confirm surface passivation, the negative potential limit was enlarged, up to the solvent reduction onset. Figure 1C (red dashed line) contains the cyclic voltammogram recorded up to -1.56 V. By forcing the solvent reaction on the freshly deposited nickel, the oxidation peak in the positive scan is almost suppressed, confirming the surface passivation.

In order to get more insights on the nickel electrodeposition on glassy carbon, chronoamperometric curves were recorded at different applied potentials (Figure 1D). All the j-t transients show an increase of the current density up to a maximum value j_m reached at a time t_m, both values (j_m,t_m) being dependent on the applied potential. By

increasing the applied potential, the current density value increases and the j_m is attained at lower t_m values. At long deposition times all the curves practically overlap. Then, the current density can be roughly considered independent on the applied potential. The profile of the whole group of j-t transients strongly suggests that the nickel deposition in the DES follows a diffusion controlled 3D nucleation and growth mechanism. It is noteworthy that the current contribution from the solvent is almost negligible under these conditions. The inset in Figure 1D contains a magnification of the j-t transients recorded from the blank solution at the different applied potential (black lines in Figure 1D). These j-t transients evidence capacitive currents. At moderate applied overpotentials, overlapping between the reduction of the solvent and the nickel deposition is not observed, in agreement with the voltammetric results. In order to confirm that the process is affected by mass transport, a j-t transient was recorded at -1.02 V under stationary conditions, and after some deposition time the solution was stirred by a constant flow of argon (Figure S2A). The current density suddenly rises when the solution is stirred until a plateau is attained, confirming the mass transport limitation. From the chronoamperometric data in Figure 1D, the diffusion coefficient of the Ni(II) in DES can be estimated by fitting the j-t transients to the Cottrell equation at $t>t_m$, i.e. by plotting j vs $1/\sqrt{t}$ (Figure S3A). Considering that the effective number of electrons transferred is 2, the calculated diffusion coefficient value D for the Ni(II) in DES was around $2.0*10^{-7}$ cm^2 s^{-1}. This value is in agreement with the previously calculated diffusion coefficients for other metallic cations in ionic liquid media.[53-55]

In order to deepen into the mechanism that governs the nickel electrodeposition on glassy carbon in the DES, the experimental j-t transients were analysed by using the non-dimensional equations formulated by Sharifker and Hills (S-H) to describe 3D

nucleation and growth mechanism, which can be progressive ($N=AN_{\infty}t$) or approach to instantaneous ($N(t)=N_{\infty}$) nucleation, respectively.[53, 55-58]

Figure 1E contains the fitting of a few j-t transients to the S-H model, i.e. by plotting j^2/j_m^2 vs t/t_m. The analysis clearly evidences the limitations of the model to describe Ni electrodeposition in DES, more specifically at longer deposition times. For the short deposition times the fittings reproduce relatively well the progressive limit, while at $t>t_m$ the fittings deviate from the model and fall below the theoretical progressive curve. Still, this analysis provides valuable information related with nucleation process at $t<t_m$, suggesting that the Ni deposition is progressive at the very early stages of the process and at moderate applied overpotentials. This progressive behaviour, however, is opposite to the results obtained in aqueous electrolytes, in which the nucleation is kinetically controlled and approach to instantaneous,[51] and also differs from some ILs in which the nucleation also tends to be instantaneous.[46, 59] These results highlight the influence of the solvent on the first steps in Ni electrodeposition. The main limitation of this classical model is precisely the fact that the formalism does not consider the solvent interactions with precursor and substrate, i.e. they neglect completely the role of the solvent. The high viscosity of the media and both solvent-substrate and solvent-precursor interactions are expected to slow down the deposition process. This fact agrees with the progressive character of the nucleation and would also explain why at $t>t_m$ (growth of the particles) the fitting appears below the theoretical curves, i.e. the growth of the deposit is kinetically hindered by the presence of the DES, specially by chloride anions which stabilize Ni(II) complexes and can adsorb on the surface.[60-62] The fact that the particular nature of the solvent influences the deposition process is not surprising. It has already been demonstrated that ILs can act as modulators of the

growth of the deposit.[29, 34, 39, 46, 48, 54, 63] To deeply analyse how the solvent affects the growth and morphology of the deposit, SEM images of the Ni deposit on glassy carbon were taken.

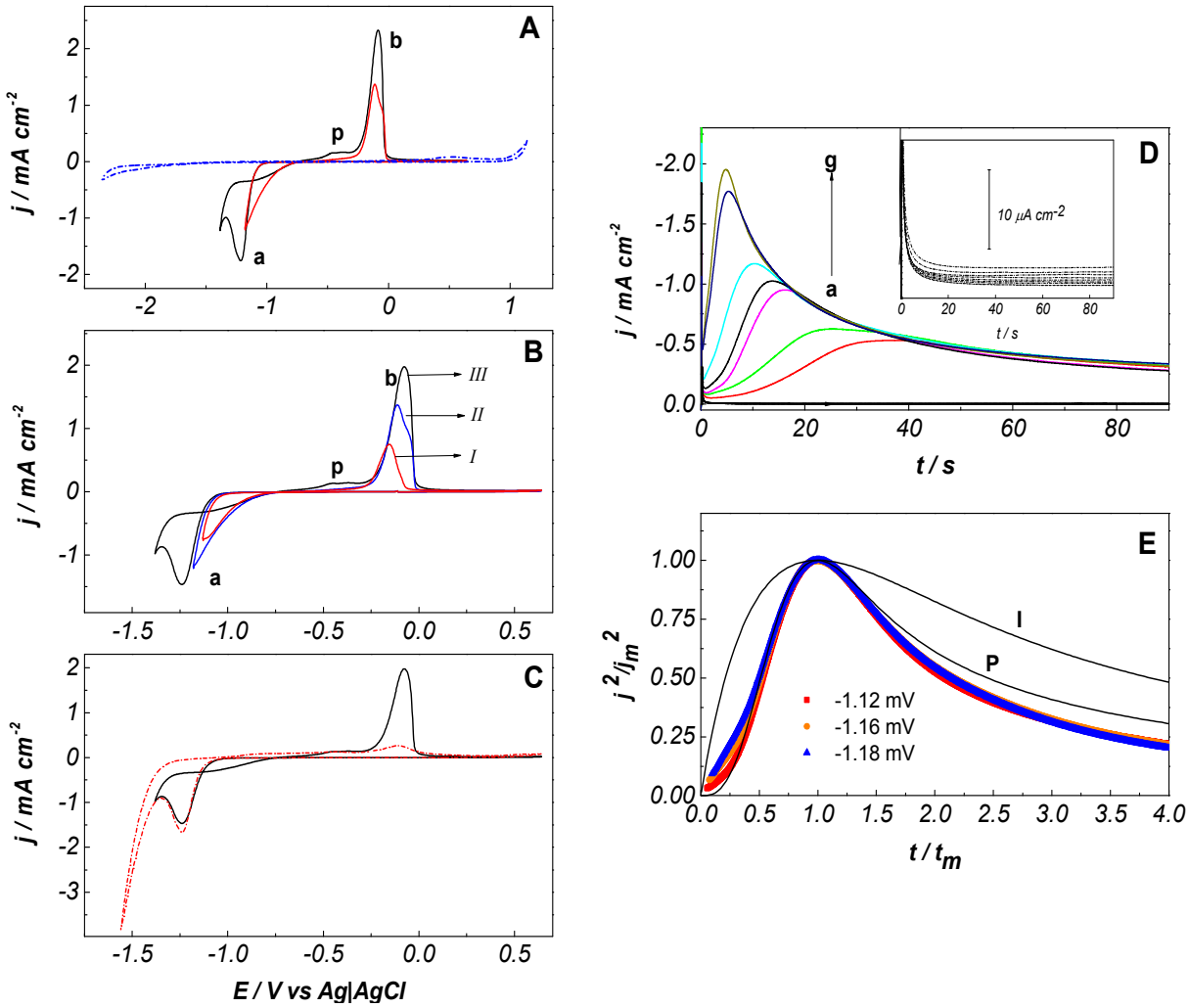

Figure 1. From 0.1 M $NiCl_2$ + DES solution and glassy carbon electrode. Cyclic voltammograms at 20 mV/s: A) dashed line) from blank solution, black solid line) wide potential limit -1.40 V and red solid line) short potential limit -1.18 V. B) at different potential limits: I) -1.13 V, II) -1.18 V and III) -1.38 V. C) at: dashed red line) -1.56 V

and black line) -1.38 V. D) j-t transients at: a) -1.07 V (red), b) -1.08 V (green), c) -1.10 V (pink), d) -1.12 V (black), e) -1.14 V (blue), f) -1.16 V (dark blue) and g) -1.18 V (brown). Black curves: j-t transients at the same potentials from the blank solution (whose magnification is in the inset). E) Non-dimensional plots according to the S-H model for some curves of Figure 1D.

Figures 2A and 2B show the FE-SEM images of nickel deposits obtained at high (E= -1.20 V) and low (E= -1.02 V) applied overpotential. The amount of circulated charge was 50 and 40 mC cm^{-2} respectively. At higher applied overpotential, Ni nanoparticles of diameter less than 100 nm were obtained, as expected from previous works.[48] By decreasing the applied overpotential (Figure 2B), Ni clusters bigger than 100 nm are formed. These clusters have also round shape, but show a clear tendency to develop cauliflower morphology due to the particle aggregation. In addition, Figure 2B shows large non covered areas of glassy carbon, result that evidences a high surface diffusion of Ni on glassy carbon, especially at lower applied overpotential. It is worth to say that no circular holes were detected on the deposit, suggesting that no solvent reduction and hydrogen formation occurs at moderate overpotentials when this specific DES is used for the electrodeposition of nickel on glassy carbon. Nanometric structures of variable size and modulation of nickel deposit is allowed in the DES by controlling the applied potential parameter. The electron dispersive X-ray spectroscopy (EDS) confirmed the presence of deposited nickel. A negligible fraction of oxygen was also detected, related to surface oxidation likely from the environment (Figure S4A). Finally, by increasing the deposition time, Ni clusters grow and aggregate forming big grains covering homogenously the entire surface (Figure S5).

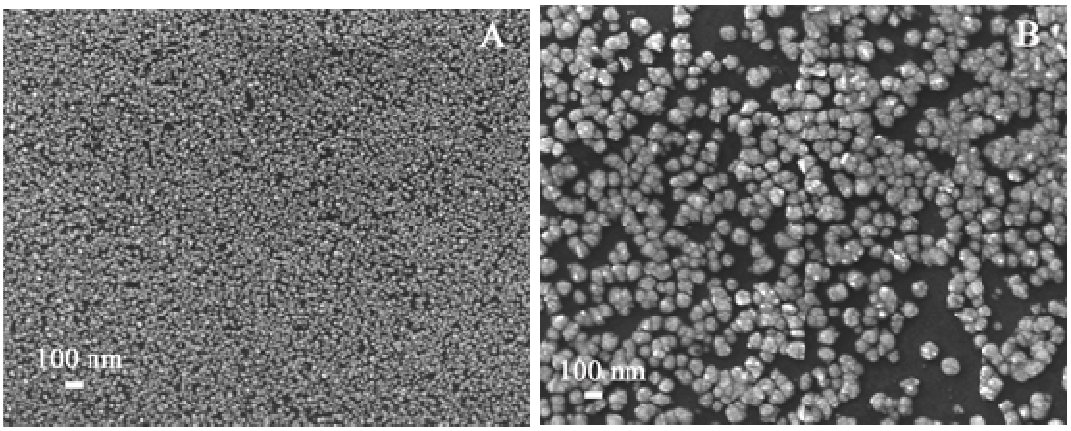

Figure 2. FE-SEM images of nickel deposits obtained from a 0.1 M $NiCl_2$ + DES solution on glassy carbon at: A) -1.20 V and 50 mC cm^{-2} and B) -1.02 V and -40 mC cm^{-2}.

This analysis shows that both solvent interaction and Ni surface diffusion influence the morphology and size of the Ni nanoparticles, which need to be considered in the analysis of the deposition mechanism on glassy carbon. Nowadays, great amount of intense efforts is put into reformulating the classical models to better rationalize the nucleation and growth mechanism. These reformulations try to introduce phenomena like surface diffusion and particles aggregation or coalescence kinetics as variables in the nucleation and growth of the particles.[48, 64-66]

Nickel electrodeposition on Pt electrode

Once analysed the nickel electrodeposition on vitreous carbon, a study on Pt surface electrode was performed to compare this process on a more reactive metallic substrate. First, a faceted platinum bead electrode, Pt(poly), was employed. This material can be considered as a model of polycrystalline surface having a regular distribution of surface

sites and compares favourably to other presentations like wires or sheets. Figure 3A shows the cyclic voltammogram for Ni electrodeposition on Pt(poly), overlapped with the blank solution. Noteworthy is that the electrochemical window recorded on Pt(poly) is considerably shorter than that on glassy carbon. Despite the narrower negative potential limit on Pt(poly), nickel electrodeposition occurs prior to solvent reduction (Figure 3A). Interesting is that the negative potential limit was widened when the Pt surface was modified by the nickel, while on glassy carbon the opposite trend was observed. This result evidences that platinum is more active towards the DES reduction than nickel, as also occurs in aqueous media.[67, 68] It is particularly remarkable that the Pt(poly)|DES oxidation scan shows a prominent oxidation peak (labelled as (z')) that has its origin in the solvent reduction. The feature increases in current density while enlarging the negative potential limit, i.e. by forcing the solvent reduction. This suggests that the peak (z') is related with the oxidation of a product generated during the solvent reduction. In order to get more insight about this feature, cyclic voltammogram was recorded in the blank solution in a narrow window. The inset of Figure 3A shows the blank voltammetric curve recorded at 50 mV s^{-1} between -1.25 V and 0.90 V. The voltammetric profile shows a double layer region between -0.20 V and 0.90 V. Previous to the massive solvent reduction, peak (z), several pairs of peaks were observed (x-x', y-y'). These voltammetric features could be related with the proton adsorption and reaction on the Pt electrode. This explanation is supported by the results obtained in protic ionic liquids where the Pt electrode displayed similar voltammetric features.[69, 70] In the present case, the hydrogen bond donor character of the urea in the DES, plus the amount of residual water, could supply the protons for the hydrogen adsorption reaction on Pt substrates in DES.[71] Then, the peak (z') would correspond to the oxidation of the hydrogen generated during the reduction of the solvent displayed in the feature (z).

The high reactivity of the Pt substrate towards the DES reduction and the hydrogen reaction could influence the nickel deposition in several ways. To investigate this, voltammetric experiments for the nickel deposition on Pt was carried at different potential limits. By scanning at lower negative potential limits, only a single oxidation peak (peak (c)) is detected in the positive scan (Figure 3B, curve I). By enlarging the cathodic potential limit, two closed reduction peaks (peaks (a) and (b)) appear (Figure 3B curve II) during the scan. Moreover, the nickel oxidation begins at more negative potentials, and the oxidation profile evolves into two overlapped features, peaks (c) and (d) (Figure 3B: curves II and III). Analogously to what occurs on glassy carbon, the solvent co-reduction causes the appearance of the current labelled previously as peak (p) and only a slight increase in intensity of the main oxidation feature (Figure 3B curve IV) is observed, evidencing the initio of some passivation process (Table S2). The scanning to -1.85 V causes the total surface passivation (Figure 3B, inset).

To demonstrate the formation of hydroxylated species while depositing Ni on Pt electrodes, XPS measures were conducted in a sample prepared by depositing Ni on Pt(poly) at -1.55 V and at -22 C cm^{-2}. Figure S6 shows the XPS multiplex between binding energies of 890 and 845 eV, and includes the Ni2p1 and Ni3p2 excitation peaks. The peaks centred at 853 eV and 870 eV correspond to metallic Ni whereas the peaks centred at 854 eV, 856 eV and 873 eV correspond to NiO_xH_y/NiO mixes. Peaks at 862 eV and 884 eV are attributed to shake up peaks (multielectron excitation).[48] The amount of NiO_xH_y/NiO is considerably higher than the amount of metallic Ni confirming the passivation phenomena at high applied potentials. Since the metallic Ni can be partially oxidized by the environment, the sample was later slightly sputtered to remove a few superficial monolayers. Figure S6B shows the XPS of the same sample

but after sputtering. Peaks related with Ni^0 now overcome those related with NiO_xH_y/NiO, but a nickel oxide or hydroxide layer is still present, confirming the passivation phenomena.

The splitting of the main oxidation feature (peaks (c) and (d)) suggests that different metallic nickel forms can be generated because of the overlapping between the nickel deposition and the solvent reaction. The overlapping with the solvent reaction would favour the formation of nickel metallic structures enriched with interstitial hydrogen in a similar way that occurs in aqueous solution. These hydrogenated structures are easier to oxidize because the presence of hydrogen in the metallic Ni bulk weakens the network. In this way, two deposited Ni forms were reported in aqueous electrolytes: α-Ni and β-Ni, being the former richer in hydrogen than the later.[51] Here, the shift of the oxidation current onset by enlarging the cathodic potential limit could evidence a transition from one hydrogenated nickel structure to another with a higher fraction of hydrogen (from α-Ni to β-Ni). To further investigate this issue, a Pt(111) single crystal was employed.

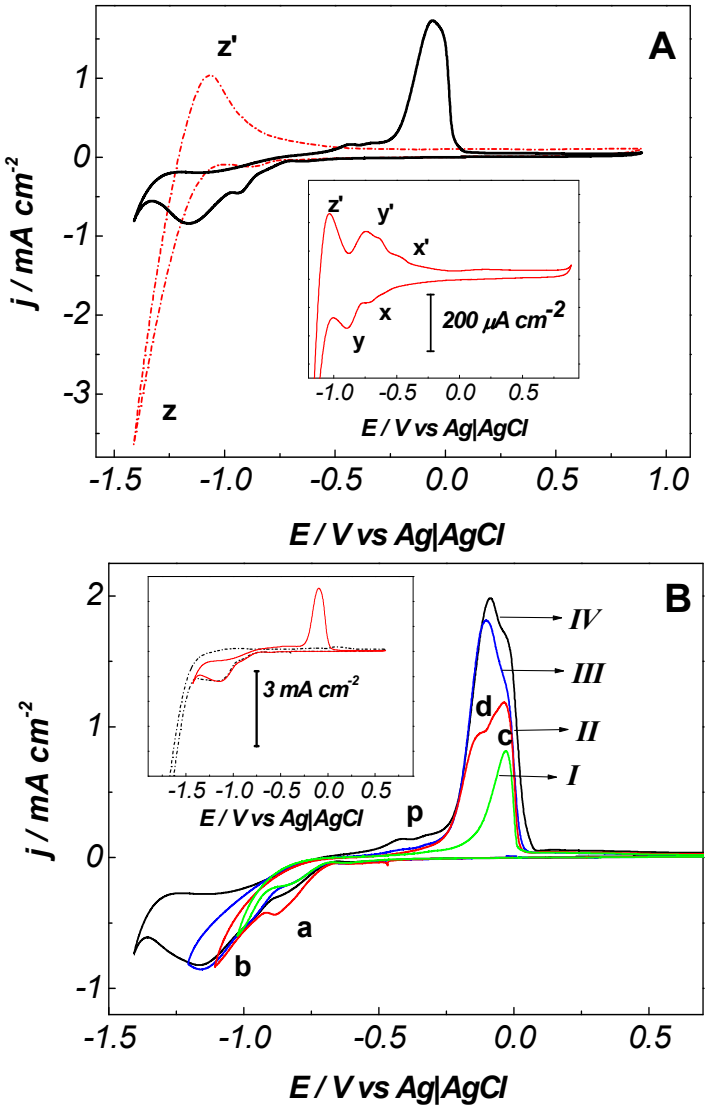

Figure 3. Cyclic voltammograms on Pt(poly) from: A) blank solution (dashed line), and 0.1M $NiCl_2$ + DES solution(black solid line). The inset shows a short voltammogram of the blank solution recorded between -1.25 V and 0.90 V at 50 mV s^{-1}. B) from the 0.1 M $NiCl_2$ + DES solution at different negative limits: I) -1.02 V, II) -1.10 V, III) -1.21 V and IV) -1.40 V. **a** and **b** are reduction peaks and **c** and **d** are oxidation peaks The inset shows potential limits of -1.40 V and -1.85 V. Scan rate 20 mV s^{-1}.

Figure 4A contains the voltammetric results for nickel deposition on Pt(111) and from the blank solution. Analogously to the Pt(poly), Pt(111) shows high activity towards the DES reduction, as evidenced by the appearance of the oxidation peak (z') in the positive scan of the blank voltammogram (dashed line). The oxidation peak (z') shows slightly lower current density than the previous one recorded on Pt(poly). The lower activity towards the hydrogen production on Pt(111) is in agreement with the results obtained in aqueous solution, evidencing some surface sensitivity to hydrogen reaction [72] related to anion adsorption and acidic effects. The blank cyclic voltammogram, recorded between -1.10 V and +0.90 V at 50mV s^{-1} (Figure 4A, inset), shows with detail the characteristic features of the Pt(111)|DES interface. The features are labelled as (x-x') and (y-y') and are slightly different than those reported on the Pt(poly), fact that can be attributed to specific adsorption. Similar to the Pt(poly), the voltammetric window is enlarged by modifying the Pt(111) surface with nickel. The nickel deposition on Pt(111) displays two peaks in the negative scan labelled as peak (a) and peak (b), suggesting a non-trivial nickel deposition mechanism. The main difference between the results obtained on Pt(111) and the Pt(poly) is that the two oxidation peaks (peaks (c) and (d)) appear more separated in the potential window on Pt(111) (Figure 4A). The voltammetric analysis shows surface sensitivity of the nickel electrodeposition on Pt substrates since the voltammetric features are better defined on Pt(111).

The origin of these two peaks was investigated by recording several cyclic voltammograms at different potential limits (Figure 4B and 4C). By reversing the scan just after reaching the first negative peak (Figure 4B, curve I), only one oxidation peak (peak (c)) is detected in the positive scan. In addition, no loop is observed in the positive scan, evidencing a strong Pt-Ni interaction. By slightly enlarging the cathodic

potential limit (Figure 4B, curve II), a shoulder centred around -0.09 V appeared in the oxidation branch, overlapped with the main oxidation peak (c). Increasing progressively the cathodic potential limit up to -1.08 V causes that the abovementioned shoulder develops into a peak labelled as (d) (Figure 4B, curves III and IV). The intensity of the peak (d) overcomes the former one (peak (c)) as the cathodic potential limit is widened. This result strongly supports that two Ni structures containing different ratios of hydrogen are formed depending on the applied potential. Higher applied overpotentials favour the highest hydrogenated Ni deposits. On the other hand, the cathodic branch of these two curves (III and IV) shows a voltammetric loop by scanning up to the first reduction peak (a). The arrows in the reduction zone in Figure 4B indicate the scan direction. The appearance of this loop in the deposition scan, just after the first reduction peak (a), suggests that the first stages of the Ni deposition on Pt(111) could involve nucleation and growth mechanism but over a Pt(111) surface covered by a few Ni monolayers instead of on the bare surface. One possibility is that the deposition mechanism follows a Stranski-Krastanov mechanism, i.e. at first some nickel monolayers grow on the surface and then the Ni nucleates and grows.[73]

Figure 4C shows the cyclic voltammograms of the Ni deposition recorded by scanning up to the reduction peak (b). As expected, when approaching the bulk solvent reduction potential, the main oxidation peaks, (peak (c) and peak (d)) both decay in intensity (Figure 4C, curves V-VII, and Table S3). In addition, the voltammogram shows the peak previously labelled as peak (p) which has increased, and a new broad band at considerable more positive potentials, labelled as peak (pp). These two peaks, peak (p) and peak (pp), are related with the initio of the surface passivation that is well evidenced

by scanning to potentials corresponding to the solvent reduction (inset Figure 4C) in a similar way that occurs on Pt(poly) substrate.

Chronoamperometric transients for the nickel deposition on Pt(111) were also recorded at different applied potentials. The j-t transients recorded at moderate and high overpotentials (between -1.0 V and -1.2 V, Figure 4D and 4E) show that the current increases until a maximum value t_m is reached. Then the current density decays by mass transport (Figure S2B). The profile of the j-t transients suggests that the nickel deposition proceeds via 3D nucleation and growth mechanism on Pt(111).[56-58] However, the j-t transients recorded between -1.05 V and -1.20 V (Figure 4D) have important dissimilarities with those recorded on glassy carbon. The most important difference is that a current non-related with 3D nucleation and growth particle overlaps with the Ni deposition at the initio of the process ($t<t_m$). One possibility is that this current is related with solvent reaction. To prove it, j-t transients within the same potential range were recorded for the Pt(111)|DES blank solution (Figure 4D, dashed lines). Current density values for blank j-t transients are too large to be only due to double layer charge and discharge, suggesting faradaic reaction of the solvent over the surface. The solvent co-reduction complicates the analysis of the data, especially at both moderate and high applied overpotentials at $t<t_m$. To minimize this solvent contribution, j-t transients were recorded at very low applied overpotential (Figure 4E). The maximum j_m value appears at considerable long deposition times, being $t_m>100$ s, illustrating how slow the process is. These transients were analysed using the S-H non-dimensional equations (Figure S7A), evidencing progressive nucleation and growth mechanism as observed on glassy carbon. However, no good fitting is found at longer times of deposition revealing the influence of the DES during the Ni deposition mechanism on Pt(111).

Spite minimizing the solvent co-reduction by decreasing the applied overpotential, there is still a current contribution that overlaps with the Ni deposition curve, and it is not related with the solvent reduction (see Figure 4D and 4E). The process linked with this current takes several seconds, from 2 s to 50 s at the lower applied overpotentials and before the nucleation and particle growth occurs. Interesting is the fact that, for similar rates of deposition, this current is almost negligible on glassy carbon, evidencing the substrate influence in the Ni electrodeposition. This lapsed time before nucleation starts is known as induction time in electrodeposition field. Traditionally, the current related with this induction time was attributed to double layer charge discharge or solvent reduction. Ustarroz et.al. reported that induction time actually would involve the formation of primary and stable clusters that act as the seeds for the nucleation and particle growth[64]. Here, in the case of Ni deposition on Pt(111), this extra current could be a reflex of 2D growth of the Ni on Pt(111) before developing stable clusters, i.e. Ni deposition following a Stranski Krastanow mechanism. The possible 2D growth before island formation is coherent with the fact that Ni-Pt interactions are much stronger than Ni-glassy carbon, so a 2D Ni growth on Pt(111) may be favoured in the very early stages of the Ni deposition.

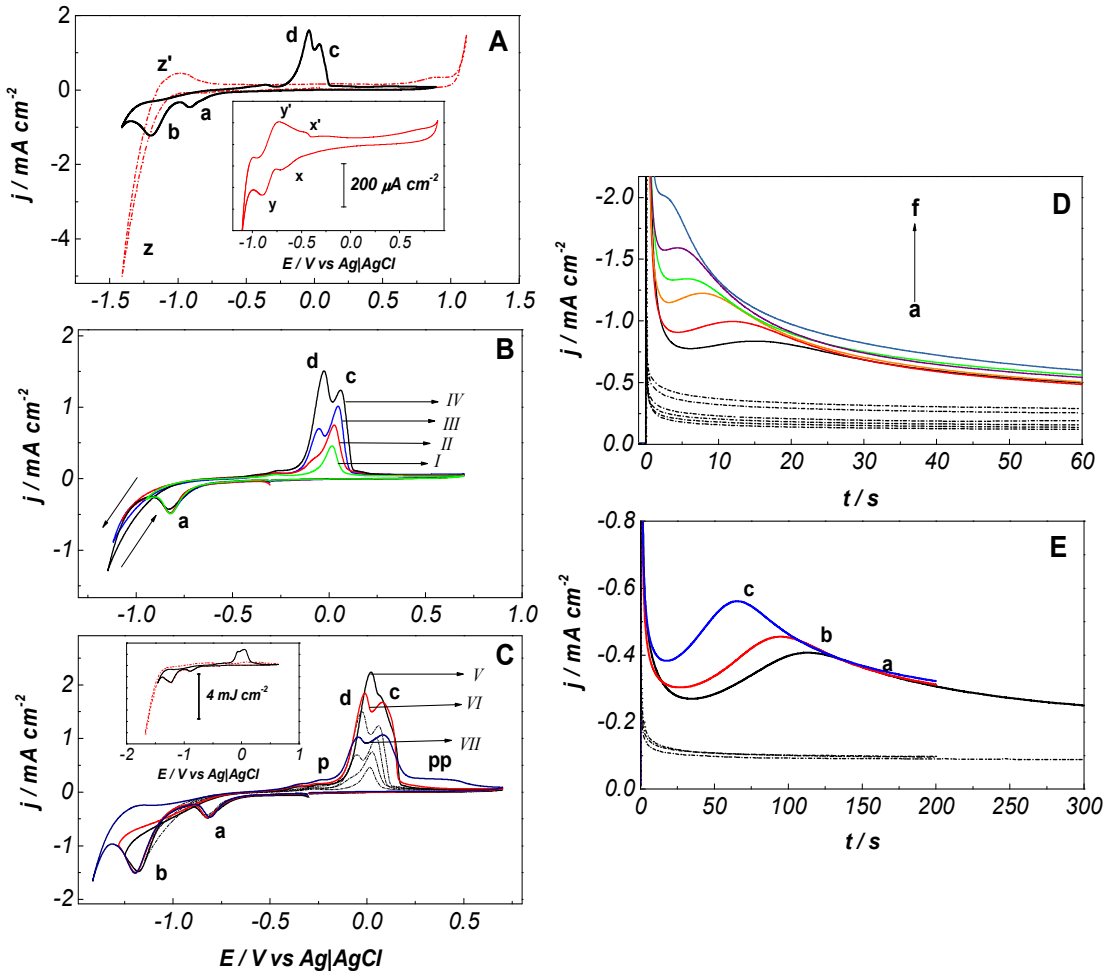

Figure 4. Pt(111) electrode. Cyclic voltammograms at 20 mV s^{-1} from: A) blank solution (red dashed line) and 0.1 M $NiCl_2$ + DES solution (black solid line). The inset shows a voltammogram from the blank solution recorded between -1.10 V and 0.90 V at 50 mV s^{-1}. B) and C) 0.1 M $NiCl_2$ + DES solution at different negative potential limits: I) -0.95 V, II) -1.08 V, III) -1.12 V, IV) -1.15 V, V) -1.25 V, VI) -1.30 V and VII) -1.42 V. Inset of C): potential limits, black line) -1.40 V and red line) -1.67 V. **a** and ***b*** are reduction peaks whereas **c** and **d** are oxidation peaks. Scan rate: 20 mV s^{-1}. D) j-t transients from: 0.1 M $NiCl_2$ + DES solution at: a) -1.08 V (black), b) -1.10 V (red), c) -1.12 V (orange), d) -1.13 V (green), e) -1.14 V (purple) and f) -1.20 V (dark blue)

and dashed lines are j-t transients recorded at the same potentials from blank solution. E) j-t transients from: 0.1 M $NiCl_2$ + DES solution at: a) -1.04 V (black), b) -1.03 V (red) and c) -1.02 V (dark blue).

In order to get additional evidence that supports the formation of hydrogenated nickel structures on Pt(111), the following experiment was carried out: before introducing the Pt(111) in the cell, the platinum surface was blocked with carbon monoxide (CO).[74, 75] For that, the electrode was flame annealed and cooled down under CO atmosphere enough time (t>60s) to ensure the whole recovery of the surface. The goal of this experiment is inhibiting the hydrogen reaction by the presence of CO. Figure 5A shows the cyclic voltammograms for the nickel deposition (solid line) and the blank solution (dashed line) both performed on the CO-Pt(111) electrode. Figure 5A also contains the cyclic voltammogram from the nickel deposition on the bare Pt(111), for comparison. When the Pt(111) is covered by CO the solvent reduction is inhibited and, consequently, the electrochemical window is enlarged. When nickel is deposited on the CO-Pt(111) substrate, the electrochemical window is shortened, due to the replacement of the CO by nickel. The presence of CO does not avoid the nickel deposition, although more overpotential is needed. The oxidation scan also displays two peaks, (peak (c) and peak (d)), but the peak (d) is more intense. These peaks appear slightly more separated in the potential window than on the bare Pt(111). Interestingly, while the peak (d) remains in the same potential position than on the bare Pt(111), the peak (c) shifts slightly to more positive potential values. This shift could be related to the CO that hinders the hydrogen formation reaction. But once replaced the CO, the hydrogen would be incorporated quickly to the nickel network as evidenced by the charge involved in peak (d).

A group of j-t transients were recorded on the CO-Pt(111) substrate at different applied potentials (Figure 5B). As expected, these j-t transients show negligible solvent contribution. All the j-t transients overlap at long deposition times allowing the calculation of the nickel (II) diffusion coefficient ($1.7*10^{-7}$ cm^2 s^{-1}, Figure S3B) that agrees with the value calculated on glassy carbon. It is worth to mention that current related with the induction time is slightly minimized when the Pt(111) is covered by CO, suggesting that CO favours the nucleation.

The j-t transients for the nickel deposition were also analysed under the formulation of the classical S-H model (Figure S7B), obtaining progressive nucleation behaviour at lower overpotentials but with a clear tendency to instantaneous nucleation by sufficiently increasing the applied overpotential.

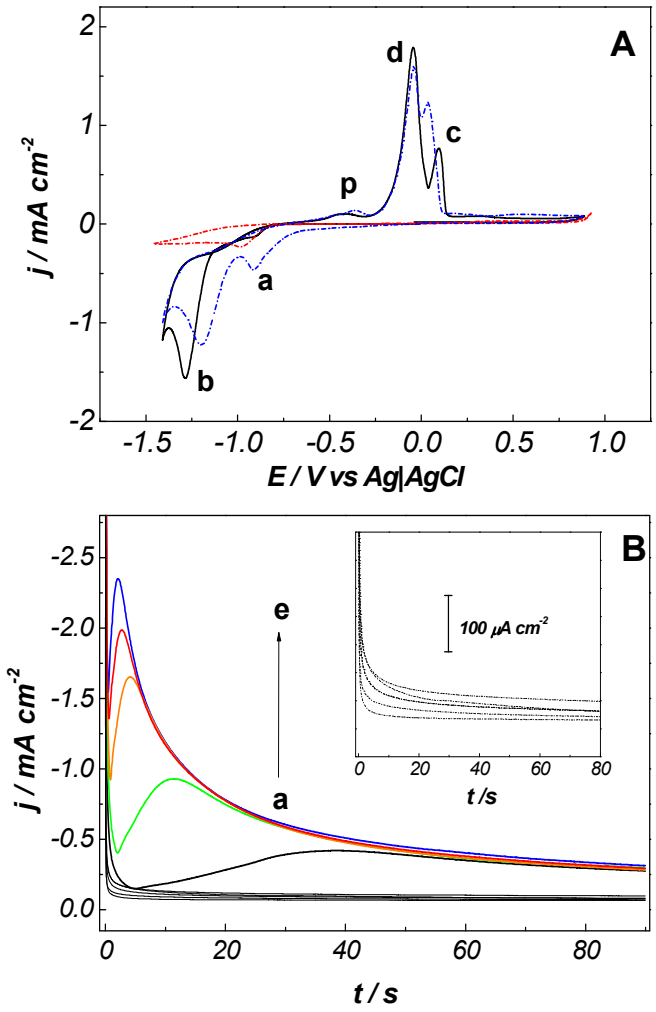

Figure 5. A) Voltammograms from 0.1 M $NiCl_2$ +DES solution: CO-Pt(111) (black solid line), bare Pt(111) (blue dashed line) and from blank solution: CO-Pt(111) (red dotted line). **a** and **b** are reduction peaks whereas **c** and **d** are oxidation peaks (Ni(II) deposition). Scan rate: 20 mV s^{-1}. B) j-t transients on CO-Pt(111) from 0.1 M $NiCl_2$ + DES solution at: a) -1.10 V (black), b) -1.125 V (green), c) -1.135 V (orange), d) -1.14 V (red) and e) -1.15 V (dark blue) and from blank solution: black lines) at the same potentials. Inset of Figure B: magnification of the j-t transients from the blank solution.

Analysis of the morphology of the Ni deposition on Pt electrodes

The voltammetric and chronoamperometric experiments provided strong evidence that the nickel deposition on Pt electrodes generates different nickel species. While at high applied overpotentials hydroxylated Ni species are favoured causing surface passivation, at moderate applied overpotential nickel structures containing interstitial hydrogen are promoted. This fraction of hydrogen can be minimized by applying even lower overpotential. Following this preliminary electrochemical analysis, we addressed the morphological and structural aspects of the nickel deposit on Pt electrodes, paying special attention to low applied overpotential.

First, the morphology of the nickel deposits on Pt(poly) electrode was analysed by FE-SEM. Samples were initially prepared at low constant overpotential during long time period in order to obtain high deposit coverages. Figure 6A contains the FE-SEM images of the obtained deposit at -0.96 V for 90 mC cm^{-2} of charge density. At higher magnification the FE-SEM image shows that the deposit has grown by developing ridge-shape crystals randomly distributed. These crystals have a size no longer than 150 nm. It is worth to say that the image back-ground can hardly be differentiated, which strongly suggests the formation of nickel nanoparticles during the first deposition times. At lower magnification (Figure 6B) a homogenous coating covering the surface is observed. However, a few large holes with radial shape are observed over some areas. These holes could be related with the formation of hydrogen bubbles on the surface promoted by platinum presence.[76] The EDS analysis confirmed the presence of nickel and a negligible fraction of oxygen was detected, supporting the non-formation at these conditions of either NiO_x or NiO_xH_y during the nickel electrodeposition (Figure S4B). To obtain more details about the nickel structures deposited on Pt(poly), XRD measures

were carried. Figure 6C contains the XRD of a nickel deposit prepared at -0.95 V on Pt(poly) substrate under a charge of -23 C cm^{-2}. The XRD confirms the presence of metallic nickel but not the presence of oxidized nickel species. The nickel deposit is polycrystalline and shows several orientations, being the most favoured the Ni(111).

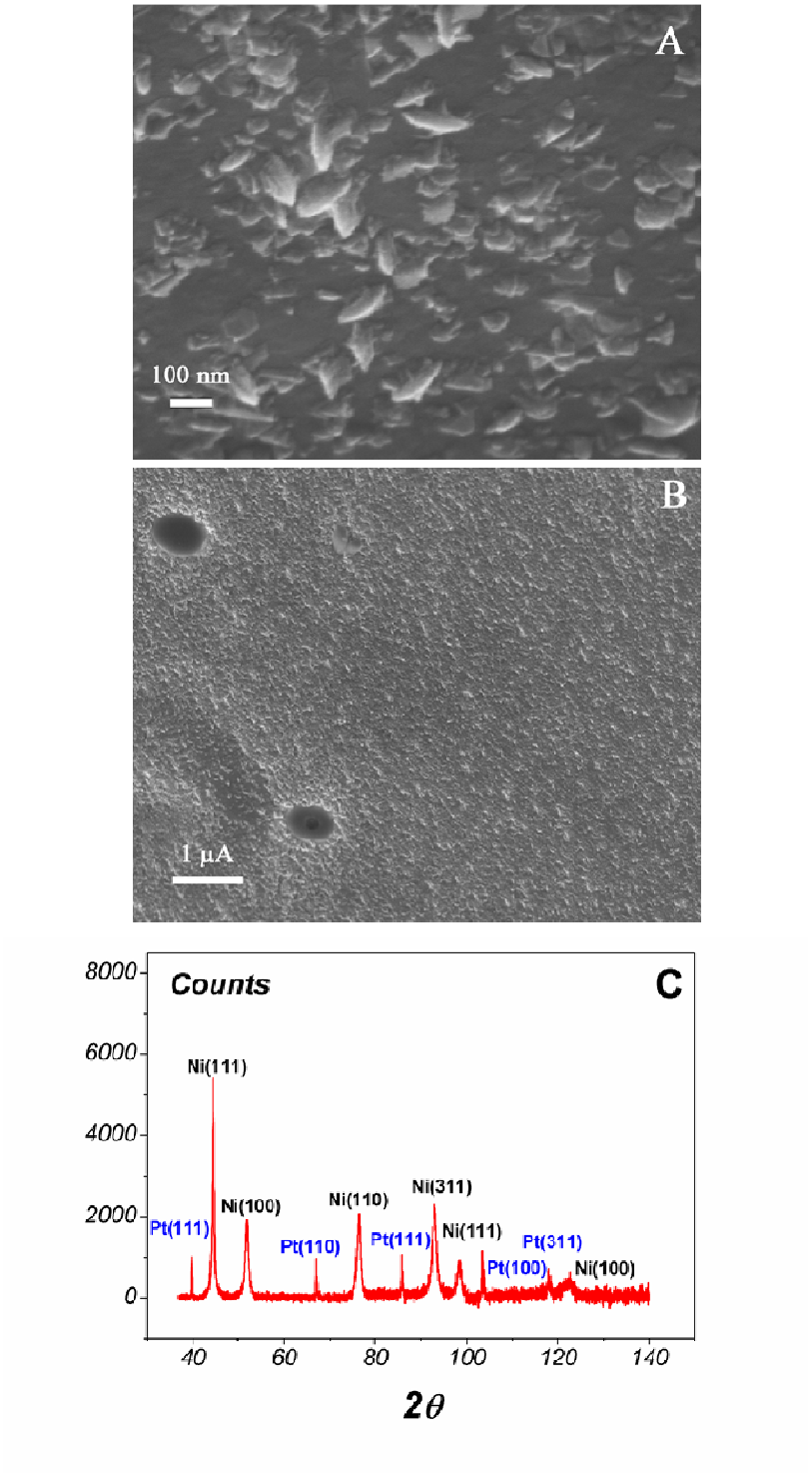

Figure 6. From 0.1 M $NiCl_2$ + DES solution and Pt(poly) electrode. A) and B) FE-SEM images of nickel deposits obtained at -0.96 V and -90 mC cm^{-2}, and C) XRD of Ni deposit obtained at -0.95 V and -23 C cm^{-2}.

The previous results on Pt(poly) have shown the morphology of the metallic nickel deposit on a Pt substrate. Then, the interest lays in elucidating if the surface orientation influences the nickel deposition. To fulfil this purpose a Pt(111) single crystal was employed. At first, the FE-SEM was carried for the bare Pt(111) surface (Figure 7A). The FE-SEM shows a flat substrate with some triangular defects that are present in the <111> orientation. The deposits were obtained by applying different potentials and after flowing an amount of charge density equal to -42 mC cm^{-2}. The FE-SEM in Figure 7B reveals the morphology of the deposit obtained on Pt(111) at high applied overpotential (-1.10 V). Rounded clusters of nanometric size which diameter is lower than 50 nm were obtained (Figure 7B). As on glassy carbon, nickel tends to grow into rounded nanoparticles. But, contrarily to the observed on glassy carbon, some circular holes appeared on the surface after carrying out the Ni deposit, supporting that co-reduction with the solvent takes place, involving production of hydrogen bubbles. By applying considerable low overpotentials, -0.98 V (Figure 7C), rounded particles were also detected, bigger than those obtained at higher applied overpotentials, as expected. However, Ni clusters deposited on Pt(111) are smaller than those obtained on glassy carbon, supporting lower surface diffusion with consequent poor particle aggregation on Pt(111). It is worth to say that at this applied potential no rounded holes were observed, reinforcing that at low applied overpotentials the hydrogen evolution reaction is minimized on Pt(111). Black triangular holes were already present on the Pt(111), as evidenced by the FE-SEM in Figure 7A. Noteworthy is that on both modified substrates the first layers of the nickel deposit have a particle size that is too small, lower than those prepared on vitreous carbon, and cannot be distinguished here. To investigate the aspect of the nickel deposit at low coverage with detail, AFM measures were performed on Pt(111) substrate using low charge densities.

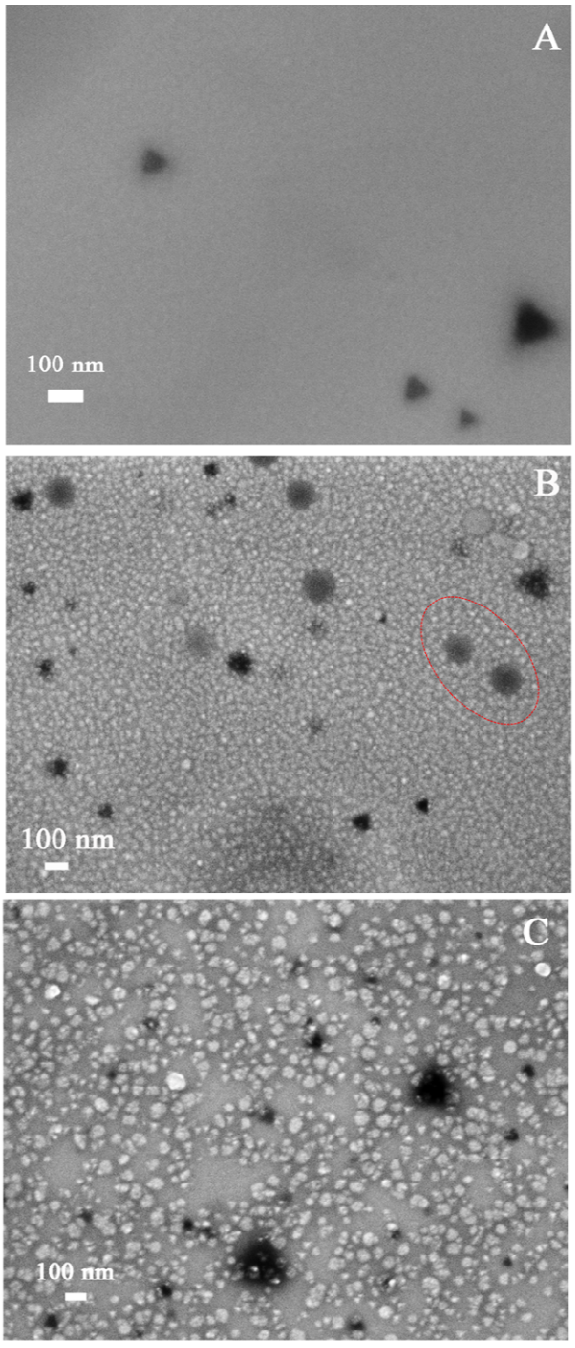

Figure 7. From Pt (111) electrode**.** FE-SEM images of: A) the bare surface of substrate. Nickel deposits obtained from 0.1 M $NiCl_2$ + DES solution at: B) -1.10 V and -42 mC cm^{-2} and C) -0.98 V and -42 mC cm^{-2}.

Figures 8A and 8B show the AFM images of Pt(111) modified by nickel obtained by applying high overpotentials (-1.12 V) and very low charge (-2 mC cm^{-2}). The AFM images clearly revealed the formation of nickel nanoparticles on the Pt(111) substrate, which diameter size is no longer than 50 nm, in agreement with FE-SEM images. As expected, the nanoparticles grow preferentially on the defects. These nanoparticles have all similar size suggesting that at this applied overpotential instantaneous nucleation may govern the deposition mechanism. In addition, the AFM shows a very thin deposit in the background rather than the bare surface. This result reinforces the idea that 2D growth takes place before growing of the particles, i.e. the deposition takes place through a Stranski-Krastanov mechanism. Figures 8C and 8D show the AFM image recorded at considerable low applied overpotential (-1.0 V) and 3 mC cm^{-2} of charge density. Here, the AFM has revealed a deposit that grows slowly forming small arrays with triangular shape. This particle distribution suggests that the triangular arrays are induced by the <111> orientation. These results strongly confirm that low applied overpotentials favour a progressive and slow growth. Rounded particles are formed which aggregate and form triangular arrays induced by the <111> orientation and favoured by the lower surface diffusion in this substrate.

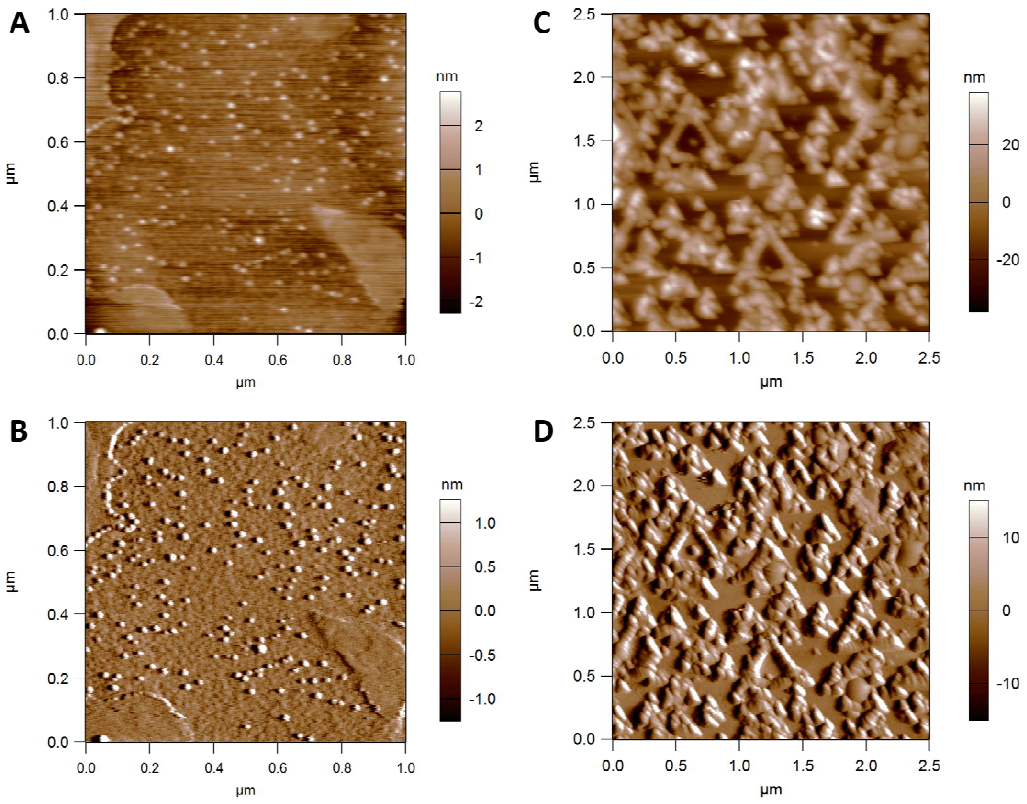

Figure 8. From a 0.1 M $NiCl_2$ + DES solution: AFM contact mode images (under MilliQ water) of: a Pt(111) surface modified by Ni deposited at -1.12 V and -2 mC cm^{-2} (1.0 x 1.0 μm^2): A) topography and B) deflection. Pt(111) surface modified by Ni deposited at -1.0 V and -3 mC cm^{-2} (2.5 x 2.5 μm^2): C) topography and D) deflection.

To get more evidence of the surface sensitivity of the Ni deposition mechanism, the Ni deposit was prepared at -2 mC cm^{-2} at the low applied overpotential, -1.0 V. Figure 9 shows clearly that the nickel grains arrange according to the atomic surface distribution of Pt(111), forming island with triangular shape, demonstrating the surface sensitivity of the nickel deposition on Pt(111) substrate. As a possible explanation, we associate these results to the high amount of chloride in the DES, besides the rest of species, which at sufficiently low applied potentials could favour the Ni ordering on the Pt(111)

according to its surface structure. Since these species adsorb and interact strongly with both the nickel and the Pt(111) substrate, they could be acting as surfactant agents.[77, 78]

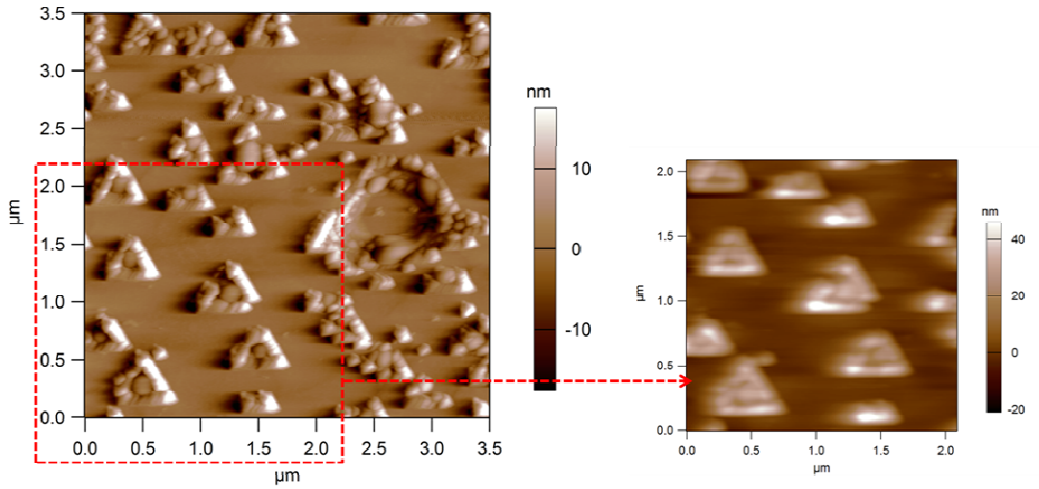

Figure 9. From a 0.1 M $NiCl_2$ + DES solution: 3.5 x 3.5 μm^2 AFM contact mode images (in air) of a Pt(111) surface modified by Ni deposited at -1.0 V and - 2mC cm^{-2}. Deflection signal and topography image of the selected area (red square).

CONCLUSIONS

The present work has deeply analysed the nickel electrodeposition on two different substrates (glassy carbon and Platinum) in a Ch:Cl/urea DES. Glassy carbon showed a wide electrochemical window that easily allowed the nickel electrodeposition. The formation of Ni deposit on glassy carbon narrowed the electrochemical window due to the enhancement of the solvent reduction by the Ni presence. Platinum electrodes, displayed an electrochemical window considerable shorter than glassy carbon, but the formation of Ni deposit enlarged their electrochemical window, evidencing that Ni is less active towards the DES reduction than Pt. On Pt, the oxidation of the Ni deposits

displayed several voltammetric peaks which current ratio is dependent on the cathodic potential limit and related to the formation of different hydrogenated Ni structures. These hydrogenated-Ni structures could be caused by the nickel co-reduction with the DES, similar to in aqueous solvents, proposal supported by the obtained chronoamperometric data. On the other hand, coupling solvent reduction with nickel reduction surface passivation was observed.

The SEM revealed the formation of rounded Ni nanoclusters on both glassy carbon and Pt(111), suggesting that this DES favours this type of morphology for the Ni deposition. For similar rates of deposition, Pt(111) induces smaller Ni clusters than those on glassy carbon, fact that could be related with the lower surface diffusion on Pt(111). While on glassy carbon the weak interaction with Ni favours the nucleation, on Pt(111) initial 2D growth could precede the island growth.

The XRD recorded on Ni-Pt(poly) modified substrate (low applied overpotential) confirmed the formation of different crystallographic orientations, but nickel oxides were not detected in any case. At higher applied overpotentials, several holes of circular shape were detected on Ni-Pt by SEM, possibly related with the formation of hydrogen bubbles during the nickel deposition. By decreasing the applied overportential, the population of holes on the deposit was minimized because of the supress of the hydrogen formation reaction on the substrate.

The AFM analysis showed that, for very low metal coverages, at high applied potentials nickel nanoparticles of similar size and homogeneously distributed are formed on Pt(111). At low applied overpotential, the nanoparticles move and form triangular arrays according to the <111> orientation.

In conclusion, the present work has shown that the ChCl/urea DES is a feasible and sustainable IL candidate to modify a metallic surface such as Pt with nanostructures of nickel. In addition, this work has shown that the nickel electrodeposition is surface sensitive in ChCl:urea DES. The high viscosity of the medium and the strong interaction between the species of the DES with precursor and substrate modulate the nickel deposition, allowing the formation of nickel nanoclusters of triangular shape on Pt(111). These studies open the possibility to use these novel solvents to synthetize new catalysts. As the DES allows modifying selectively the substrate, the preparation of high catalytic surfaces such as Pt with low amounts of other metals could be tailored, deposition process that, on the other hand, is difficult to perform in aqueous solvents.

ASSOCIATED CONTENT

Supporting Information.

This material is available free of charge via the Internet at http://pubs.acs.org.

Blank Cyclic voltammograms of Pt(poly)| DES with different amounts of water; Tables containing the Q_{ox} and Q_{red} charge values for voltammetric curves related with the Ni deposition; j-t transients recorded under stirred conditions on both glassy carbon and Pt(111) substrates; linearization of a few j-t transients recorded on glassy carbon and CO-Pt(111); EDS spectra of the Ni deposits on both glassy carbon and Pt(poly); SEM image of Ni deposited on glassy carbon at high coverage; XPS of a Ni-Pt(poly) sample prepared at high applied overpotential; fitting to the S-H model of a few j-t transients recorded on both Pt(111) and CO-Pt(111) substrates.

AUTHOR INFORMATION

Corresponding Author

*E-mail: e.gomez@ub.edu

*E-mail: j.feliu@ua.es

ORCID

Elvira Gómez: 0000-0002-9223-6357

Juan Feliu: 0000-0003-4751-3279

Author Contributions

The manuscript was written through contributions of all authors. All authors have given approval to the final version of the manuscript.

Notes

The authors declare no competing financial interest.

ACKNOWLEDGMENTS

This work has been financially supported by the MCINN-FEDER (Spain) through the projects: CTQ2016-76221-P and TEC2014-51940-C2-2R. P. Sebastian acknowledges to MECD the award of a FPU grant.

REFERENCES

(1) Faulkner, A. J. B. a. L. R., *Electrochemical Methods. Fundamentals and Applications*. 2nd ed.; Wiley: New York, 2001; p.850.

(2) Srimathi, S. N.; Mayanna, S. M.; Sheshadri, B. S., Electrodeposition of Binary Magnetic Alloys. *Surf. Technol.* **1982,** *16*, 277-322.

(3) Liu, D. M.; Cong, D. Y.; Sun, X. M.; Chen, H. Y.; Nie, Z. H.; Chen, Z.; Zhang, Y.; Zhu, C.; Qu, Y. H.; Zhu, J.; Wang, Y. D., Low-Hysteresis Tensile Superelasticity in a Ni-Co-Mn-Sn

Magnetic Shape Memory Microwire. *J. Alloy. Compd.* **2017,** *728* (Supplement C), 655-658.

(4) Avci, C. O.; Mann, M.; Tan, A. J.; Gambardella, P.; Beach, G. S. D., A Multi-State Memory Device Based on the Unidirectional Spin Hall Magnetoresistance. *Appl. Phys. Lett.* **2017,** *110*, 203506.

(5) Kinoshita, K.; Makino, T.; Yoda, T.; Dobashi, K.; Kishida, S., Analysis on Data Storage Area of NiO-ReRAM with Secondary Electron Image. *J. Mater. Res.* **2011,** *26*, 45-49.

(6) Lee, M.-J.; Ahn, S.-E.; Lee, C. B.; Kim, C.-J.; Jeon, S.; Chung, U. I.; Yoo, I.-K.; Park, G.-S.; Han, S.; Hwang, I. R.; Park, B.-H., A Simple Device Unit Consisting of All NiO Storage and Switch Elements for Multilevel Terabit Nonvolatile Random Access Memory. *ACS Appl. Mater. Inter.* **2011,** *3*, 4475-4479.

(7) Debashis, P.; Achintya, D.; Samit, K. R., Improved Charge Storage Characteristics of the Tetralayer Non-Volatile Memory Structure using Nickel Nanocrystal Trapping Layer. *Semicond. Sci. Tech.* **2009,** *24*, 115020.

(8) Casals-Terré, J.; Duch, M.; Plaza, J. A.; Esteve, J.; Pérez-Castillejos, R.; Vallés, E.; Gómez, E., Design and Characterization of a Magnetic Digital Flow Regulator. *Sensor Actuator. A: Physical* **2010,** *162*, 107-115.

(9) Lucas, I.; Michelena, M. D.; del Real, R. P.; de Manuel, V.; Plaza, J. A.; Duch, M.; Esteve, J.; Guerrero, H., A New Single-Sensor Magnetic Field Gradiometer. *Sens. Lett.* **2009,** *7*, 563-570.

(10) Rinaldi, A. L.; Carballo, R., Impedimetric Non-Enzymatic Glucose Sensor Based on Nickel Hydroxide Thin Film onto Gold Electrode. *Sensor. Actuator. B-Chem.* **2016,** *228*, 43-52.

(11) Trotochaud, L.; Young, S. L.; Ranney, J. K.; Boettcher, S. W., Nickel–Iron Oxyhydroxide Oxygen-Evolution Electrocatalysts: The Role of Intentional and Incidental Iron Incorporation. *J. Am. Chem. Soc.* **2014,** *136*, 6744-6753.

(12) Diaz-Morales, O.; Ledezma-Yanez, I.; Koper, M. T. M.; Calle-Vallejo, F., Guidelines for the Rational Design of Ni-Based Double Hydroxide Electrocatalysts for the Oxygen Evolution Reaction. *ACS Catal.* **2015,** *5*, 5380-5387.

(13) Diaz-Morales, O.; Ferrus-Suspedra, D.; Koper, M. T. M., The Importance of Nickel Oxyhydroxide Deprotonation on its Activity Towards Electrochemical Water Oxidation. *Chem. Sci.* **2016,** *7*, 2639-2645.

(14) Subbaraman, R.; Tripkovic, D.; Chang, K. C.; Strmcnik, D.; Paulikas, A. P.; Hirunsit, P.; Chan, M.; Greeley, J.; Stamenkovic, V.; Markovic, N. M., Trends in Activity for the Water Electrolyser Reactions on 3d M(Ni,Co,Fe,Mn) Hydr(oxy)oxide Catalysts. *Nat. Mat.* **2012,** *11*, 550-557.

(15) Subbaraman, R.; Tripkovic, D.; Strmcnik, D.; Chang, K. C.; Uchimura, M.; Paulikas, A. P.; Stamenkovic, V.; Markovic, N. M., Enhancing Hydrogen Evolution Activity in Water Splitting by Tailoring Li^+-$Ni(OH)_2$-Pt Interfaces. *Science* **2011,** *334*, 1256-1260.

(16) Ledezma-Yanez, I.; Wallace, W. D. Z.; Sebastián-Pascual, P.; Climent, V.; Feliu, J. M.; Koper, M. T. M., Interfacial Water Reorganization as a pH-Dependent Descriptor of the Hydrogen Evolution Rate on Platinum Electrodes. *Nat. Energy* **2017,** *2, 17031*.

(17) Tamašauskaitė-Tamašiūnaitė, L.; Balčiūnaitė, A.; Vaiciukevičienė, A.; Selskis, A.; Pakštas, V., Investigation of Nanostructured Platinum–Nickel Supported on the Titanium Surface as Electrocatalysts for Alkaline Fuel Cells. *J. Power Sources* **2012,** *208* (Supplement C), 242-247.

(18) Fleischmann, M.; Korinek, K.; Pletcher, D., The Oxidation of Organic Compounds at a Nickel Anode in Alkaline Solution. *J. Electroanal. Chem.* **1971,** *31*, 39-49.

(19) Gong, M.; Wang, D.-Y.; Chen, C.-C.; Hwang, B.-J.; Dai, H., A Mini Review on Nickel-Based Electrocatalysts for Alkaline Hydrogen Evolution Reaction. *Nano Res.* **2016,** *9*, 28-46.

(20) Toda, T.; Igarashi, H.; Uchida, H.; Watanabe, M., Enhancement of the Electroreduction of Oxygen on Pt Alloys with Fe, Ni, and Co. *J. Electrochem. Soc.* **1999,** *146*, 3750-3756.

(21) Stamenkovic, V. R.; Fowler, B.; Mun, B. S.; Wang, G.; Ross, P. N.; Lucas, C. A.; Markovic, N. M., Improved Oxygen Reduction Activity on $Pt_3Ni(111)$ Via Increased Surface Site Availability. *Science* **2007,** *315*, 493-497.

(22) Serrà, A.; Gimeno, N.; Gomez, E.; Mora, M.; Sagrista, M. L.; Valles, E., Magnetic Mesoporous Nanocarriers for Drug Delivery with Improved Therapeutic Efficacy. *Adv. Funct. Mater.* **2016,** *26*, 6601-6611.

(23) Dini, J. W., Electrodeposition. The material Science of Coatings and Substrates. 1st ed.; publications, N., Ed. Advanced Materials, Noyes Publication, New York, 1993; 367.

(24) Fleischmann, M., Saraby-Reintjes, A., The Simultaneous Deposition of Nickel and Hydrogen on Vitreous Carbon. *Electrochim. Acta* **1984,** *29*, 69-75.

(25) Su, Y. Z.; Fu, Y. C.; Wei, Y. M.; Yan, J. W.; Mao, B. W., The Electrode/Ionic Liquid Interface: Electric Double Layer and Metal Electrodeposition. *ChemPhysChem* **2010,** *11*, 2764-2778.

(26) Buzzeo, M. C.; Evans, R. G.; Compton, R. G., Non-Haloaluminate Room-Temperature Ionic Liquids in Electrochemistry—A Review. *ChemPhysChem* **2004,** *5*, 1106-1120.

(27) Katayama, Y., Electrodeposition of Metals in Ionic Liquids. In *Electrochemical Aspects of Ionic Liquids*, John Wiley &Sons, New Jersey, 2005; 111-131.

(28) Frank Endres, D. R. M., Andrew Abbott, *Electrodeposition from Ionic Liquids*. 2nd ed.; Wiley, New York, 2017; p 486.

(29) Zhang, Q.; Wang, Q.; Zhang, S.; Lu, X.; Zhang, X., Electrodeposition in Ionic Liquids. *ChemPhysChem* **2016,** *17*, 335-351.

(30) Zhu, Y. L.; Katayama, Y.; Miura, T. In *Electrochemical Preparation of Nickel and Iron Nanoparticles in a Hydrophobic Ionic Liquid*, ECS Transactions, **2010**, 6, 537-541.

(31) Zhu, Y. L.; Katayama, Y.; Miura, T., Electrochemical Co-Deposition of Iron and Nickel from a Hydrophobic Ionic Liquid. *J. Electrochem. Soc.* **2015,** *162*, D371-D375.

(32) Zhu, Y. L.; Katayama, Y.; Miura, T., Effects of Acetonitrile on Electrodeposition of Ni from a Hydrophobic Ionic Liquid. *Electrochim. Acta* **2010,** *55*, 9019-9023.

(33) Zhu, Y. L.; Katayama, Y.; Miura, T., Effects of Acetone and Thiourea on Electrodeposition of Ni from a Hydrophobic Ionic Liquid. *Electrochim. Acta* **2012,** *85*, 622-627.

(34) Liu, Z.; Cui, T.; Pulletikurthi, G.; Lahiri, A.; Carstens, T.; Olschewski, M.; Endres, F., Dendrite-Free Nanocrystalline Zinc Electrodeposition from an Ionic Liquid Containing Nickel Triflate for Rechargeable Zn-Based Batteries. *Angew. Chem. Int. Edit.* **2016,** *55*, 2889-2893.

(35) Smith, E. L.; Abbott, A. P.; Ryder, K. S., Deep Eutectic Solvents (DESs) and Their Applications. *Chem. Rev.* **2014,** *114*, 11060-11082.

(36) Abbott, A. P.; Boothby, D.; Capper, G.; Davies, D. L.; Rasheed, R. K., Deep Eutectic Solvents Formed Between Choline Chloride and Carboxylic Acids: Versatile Alternatives to Ionic Liquids. *J. Am. Chem. Soc.* **2004,** *126*, 9142-9147.

(37) Abbott, A. P.; Capper, G.; Davies, D. L.; Munro, H. L.; Rasheed, R. K.; Tambyrajah, V., Preparation of Novel, Moisture-Stable, Lewis-Acidic Ionic Liquids Containing Quaternary Ammonium Salts with Functional Side Chains. *Chem. Commun.* **2001,** 2010-2011.

(38) Abbott, A. P.; Ballantyne, A.; Harris, R. C.; Juma, J. A.; Ryder, K. S.; Forrest, G., A Comparative Study of Nickel Electrodeposition Using Deep Eutectic Solvents and Aqueous Solutions. *Electrochim. Acta* **2015,** *176*, 718-726.

(39) Gu, C.; Tu, J., One-Step Fabrication of Nanostructured Ni Film with Lotus Effect from Deep Eutectic Solvent. *Langmuir* **2011,** *27*, 10132-10140.

(40) Du, C.; Zhao, B.; Chen, X.-B.; Birbilis, N.; Yang, H., Effect of Water Presence on Choline Chloride-2Urea Ionic Liquid and Coating Platings from the Hydrated Ionic Liquid. Sci. Rep. **2016,** *6*, 29225.

(41) Bernasconi, R.; Magagnin, L., Electrodeposition of Nickel from DES on Aluminium for Corrosion Protection. *Surface. Engineering.* **2017,** *33*, 131-135.

(42) Abbott, A. P.; El Ttaib, K.; Ryder, K. S.; Smith, E. L., Electrodeposition of Nickel using Eutectic Based Ionic Liquids. *Transactions of the IMF* **2008,** *86*, 234-240.

(43) Florea, A.; Anicai, L.; Costovici, S.; Golgovici, F.; Visan, T., Ni and Ni Alloy Coatings Electrodeposited from Choline Chloride-Based Ionic Liquids - Electrochemical Synthesis and Ccharacterization. *Surf. Interface Anal.* **2010,** *42*, 1271-1275.

(44) Yang, H.; Guo, X.; Birbilis, N.; Wu, G.; Ding, W., Tailoring Nickel Coatings Via Electrodeposition from a Eutectic-Based Ionic Liquid Doped with Nicotinic Acid. *Appl. Surf. Science* **2011,** *257*, 9094-9102.

(45) Gu, C. D.; Zhang, J. L.; Bai, W. Q.; Tong, Y. Y.; Wang, X. L.; Tu, J. P., Electro-Brush Plating from Deep Eutectic Solvent: A Case of Nanocrystalline Ni Coatings with Superior Mechanical Property and Corrosion Resistance. *J. Electrochem. Soc.* **2015,** *162*, D159-D165.

(46) You, Y.; Gu, C.; Wang, X.; Tu, J., Electrochemical Synthesis and Characterization of Ni-P Alloy Coatings from Eutectic-Based Ionic Liquid. *J. Electrochem. Soc.* **2012,** *159*, D642-D648.

(47) You, Y. H.; Gu, C. D.; Wang, X. L.; Tu, J. P., Electrodeposition of Ni-Co Alloys from a Deep Eutectic Solvent. *Surf. Coat. Technol.* **2012,** *206*, 3632-3638.

(48) Mernissi Cherigui, E. A.; Sentosun, K.; Bouckenooge, P.; Vanrompay, H.; Bals, S.; Terryn, H.; Ustarroz, J., Comprehensive Study of the Electrodeposition of Nickel Nanostructures from Deep Eutectic Solvents: Self-Limiting Growth by Electrolysis of Residual Water. *J. Phys. Chem. C* **2017,** *121*, 9337-9347.

(49) Clavilier, J., The Role of Anion on the Electrochemical Behaviour of a {111} Platinum Surface; an Unusual Splitting of the Voltammogram in the Hydrogen Region. *J. Electroanal. Chem.* **1979,** *107*, 211-216.

(50) Gómez, E.; Cojocaru, P.; Magagnin, L.; Valles, E., Electrodeposition of Co, Sm and SmCo from a Deep Eutectic Solvent. *J. Electroanal. Chem.* **2011,** *658*, 18-24.

(51) Gómez, E.; Pollina, R.; Vallés, E., Nickel Electrodeposition on Different Metallic Substrates. *J. Electroanal. Chem.* **1995,** *386*, 45-56.

(52) Matulis, J.; Sližys, R., On some Characteristics of Cathodic Processes in Nickel Electrodeposition. *Electrochim. Acta* **1964,** *9*, 1177-1188.

(53) Sebastián, P.; Torralba, E.; Vallés, E.; Molina, A.; Gómez, E., Advances in Copper Electrodeposition in Chloride Excess. A Theoretical and Experimental Approach. *Electrochim. Acta* **2015,** *164*, 187-195.

(54) Abbott, A. P.; El Ttaib, K.; Frisch, G.; McKenzie, K. J.; Ryder, K. S., Electrodeposition of Copper Composites from Deep Eutectic Solvents Based on Choline Chloride. *Phys. Chem. Chem. Phys.* **2009,** *11*, 4269-4277.

(55) Sebastián, P.; Botello, L. E.; Vallés, E.; Gómez, E.; Palomar-Pardavé, M.; Scharifker, B. R.; Mostany, J., Three-Dimensional Nucleation with Diffusion Controlled Growth: A Comparative Study of Electrochemical Phase Formation from Aqueous and Deep Eutectic Solvents. *J. Electroanal. Chem.* **2016,** *793*,119-125.

(56) Scharifker, B.; Hills, G., Theoretical and Experimental Studies of Multiple Nucleation. *Electrochim. Acta* **1983,** *28*, 879-889.
(57) Gunawardena, G.; Hills, G.; Montenegro, I.; Scharifker, B., Electrochemical Nucleation. Part I. General Considerations. *J. Electroanal. Chem.* **1982,** *138*, 225-239.
(58) Gunawardena, G.; Hills, G.; Montenegro, I., Electrochemical Nucleation. *Journal of Electroanal. Chem.* **1985,** *184*, 357-369.
(59) Zhu, Y. L.; Kozuma, Y.; Katayama, Y.; Miura, T., Electrochemical Behavior of Ni(II)/Ni in a Hydrophobic Amide-Type Room-Temperature Ionic Liquid. *Electrochim. Acta* **2009,** *54*, 7502-7506.
(60) Abbott, A. P.; Barron, J. C.; Frisch, G.; Gurman, S.; Ryder, K. S.; Fernando Silva, A., Double Layer Effects on Metal Nucleation in Deep Eutectic Solvents. *Phys.l Chem. Chem. Phys.* **2011,** *13*, 10224-10231.
(61) Abbott, A. P.; McKenzie, K. J., Application of Ionic Liquids to the Electrodeposition of Metals. *Phys. Chem. Chem. Phys.* **2006,** *8*, 4265-4279.
(62) Hartley, J. M.; Ip, C.-M.; Forrest, G. C. H.; Singh, K.; Gurman, S. J.; Ryder, K. S.; Abbott, A. P.; Frisch, G., EXAFS Study into the Speciation of Metal Salts Dissolved in Ionic Liquids and Deep Eutectic Solvents. *Inorg. Chem.* **2014,** *53*, 6280-6288.
(63) Gu, C. D.; You, Y. H.; Yu; Y. L.; Qu; S. X.; Tu, J. P. Microstructure, Nanoindentation, and Electrochemical Properties of the Nanocrystalline Nickel Film Electrodeposited from Choline chloride–Ethylene Glycol. *Surf. Coat. Tech.* **2011,** *205*, 4928-4933.
(64) Ustarroz, J.; Hammons, J. A.; Altantzis, T.; Hubin, A.; Bals, S.; Terryn, H., A Generalized Electrochemical Aggregative Growth Mechanism. *J. Am. Chem. Soc.* **2013,** *135*, 11550-11561.
(65) Ustarroz, J.; Ke, X.; Hubin, A.; Bals, S.; Terryn, H., New Insights into the Early Stages of Nanoparticle Electrodeposition. *J. Phys. Chem. C* **2012,** *116*, 2322-2329.
(66) Manh, T. L.; Arce-Estrada, E. M.; Romero-Romo, M.; Mejía-Caballero, I.; Aldana-González, J.; Palomar-Pardavé, M., On Wetting Angles and Nucleation Energies during the Electrochemical Nucleation of Cobalt onto Glassy Carbon from a Deep Eutectic Solvent. *J. Electrochem. Soc.* **2017,** *164*, D694-D699.
(67) Laursen, A. B.; Varela, A. S.; Dionigi, F.; Fanchiu, H.; Miller, C.; Trinhammer, O. L.; Rossmeisl, J.; Dahl, S., Electrochemical Hydrogen Evolution: Sabatier's Principle and the Volcano Plot. *Journal of Chemical Education* **2012,** *89*, 1595-1599.
(68) Skúlason, E.; Tripkovic, V.; Björketun, M. E.; Gudmundsdóttir, S.; Karlberg, G.; Rossmeisl, J.; Bligaard, T.; Jónsson, H.; Nørskov, J. K., Modeling the Electrochemical Hydrogen Oxidation and Evolution Reactions on the Basis of Density Functional Theory Calculations. *J. Phys. Chem. C* **2010,** *114*, 18182-18197.
(69) Ejigu, A.; Walsh, D. A., The Role of Adsorbed Ions during Electrocatalysis in Ionic Liquids. *J. Phys. Chem. C* **2014,** *118*, 7414-7422.
(70) Johnson, L.; Ejigu, A.; Licence, P.; Walsh, D. A., Hydrogen Oxidation and Oxygen Reduction at Platinum in Protic Ionic Liquids. *J. Phys. Chem. C* **2012,** *116*, 18048-18056.
(71) Abbott, A. P.; Capper, G.; Davies, D. L.; Rasheed, R. K.; Tambyrajah, V., Novel Solvent Properties of Choline Chloride/Urea Mixtures. *Chem. Commun.* **2003,** 70-71.
(72) Conway, B. E.; Tilak, B. V., Interfacial Processes Involving Electrocatalytic Evolution and Oxidation of H2, and the Role of Chemisorbed H. *Electrochim. Acta* **2002,** *47*, 3571-3594.
(73) Danilov, A. I.; Molodkina, E. B.; Rudnev, A. V.; Polukarov, Y. M.; Feliu, J. M., Kinetics of Copper Deposition on Pt(111) and Au(111) Electrodes in Solutions of Different Acidities. *Electrochim. Acta* **2005,** *50*, 5032-5043.

(74) Kibler, L. A.; Cuesta, A.; Kleinert, M.; Kolb, D. M., In-situ STM Characterisation of the Surface Morphology of Platinum Single Crystal Electrodes as a Function of their Preparation. *J. Electroanal. Chem.* **2000,** *484*, 73-82.

(75) Feliu, J. M.; Orts, J. M.; Gómez, R.; Aldaz, A.; Clavilier, J., New Information on the Unusual Adsorption States of Pt(111) in Sulphuric Acid Solutions from Potentiostatic Adsorbate Replacement by CO. *J. Electroanal. Chem.* **1994,** *372*, 265-268.

(76) Garrido, P.; Gómez, E.; Vallés, E., Simultaneous Electrodeposition and Detection of Platinum on Silicon Surfaces. *J. Electroanal. Chem.* **1998,** *441*, 147-151.

(77) Chen, W.; Yen, P.; Kuo, Y.; Chen, S.; Yau, S., Epitaxial Electrodeposition of Nickel on Pt(111) Electrode. *J. Phys. Chem. C* **2012,** *116*, 21343-21349.

(78) Sebastián, P.; Gómez, E.; Climent, V.; Feliu, J. M., Copper Underpotential Deposition at Gold Surfaces in Contact with a Deep Eutectic Solvent: New Insights. *Electrochem. Commun.* **2017,** *78*, 51-55.

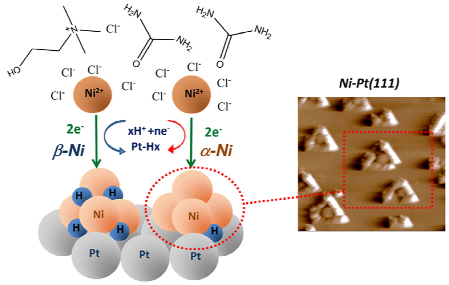

For Table of Contents Only

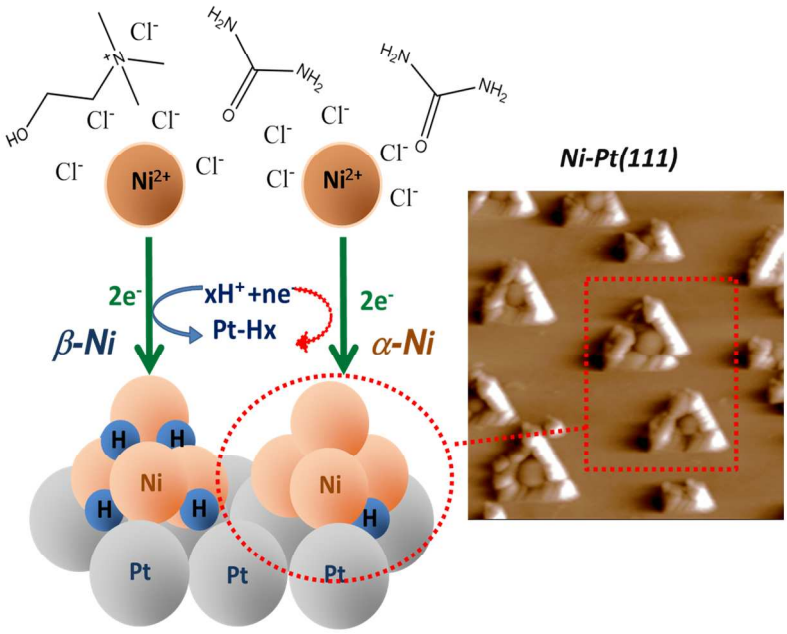

Scheme 1

Scheme 1. Ni(II) electrodeposition in DES on Pt(111) and AFM of the Ni clusters

1000x800mm (78 x 78 DPI)

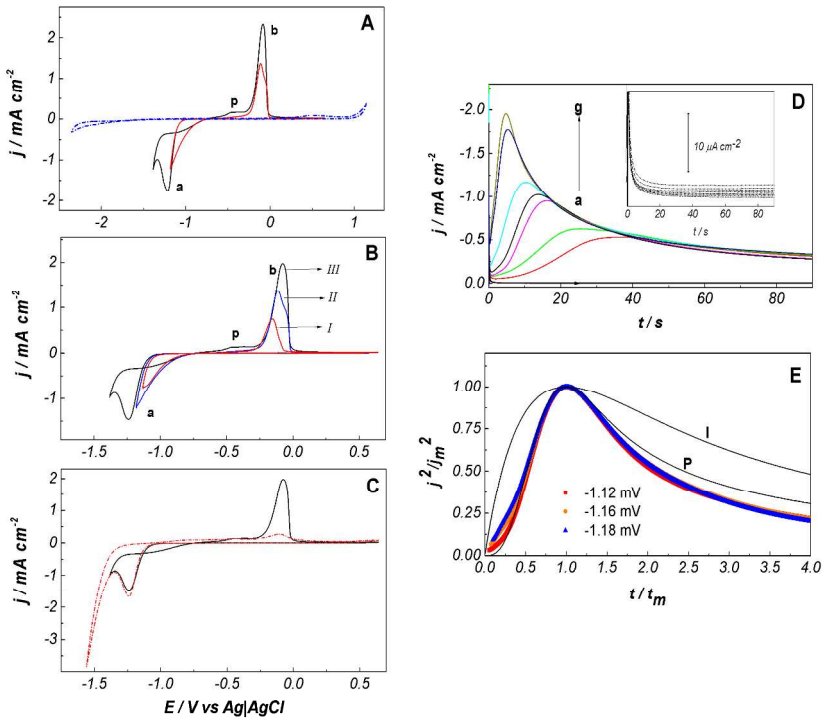

Figure 1

Figure 1

1000x800mm (78 x 78 DPI)

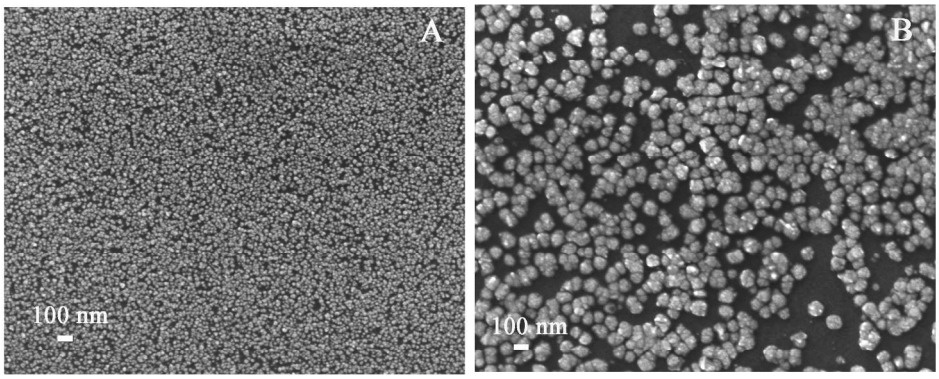

Figure 2

Figure 2

1300x753mm (60 x 60 DPI)

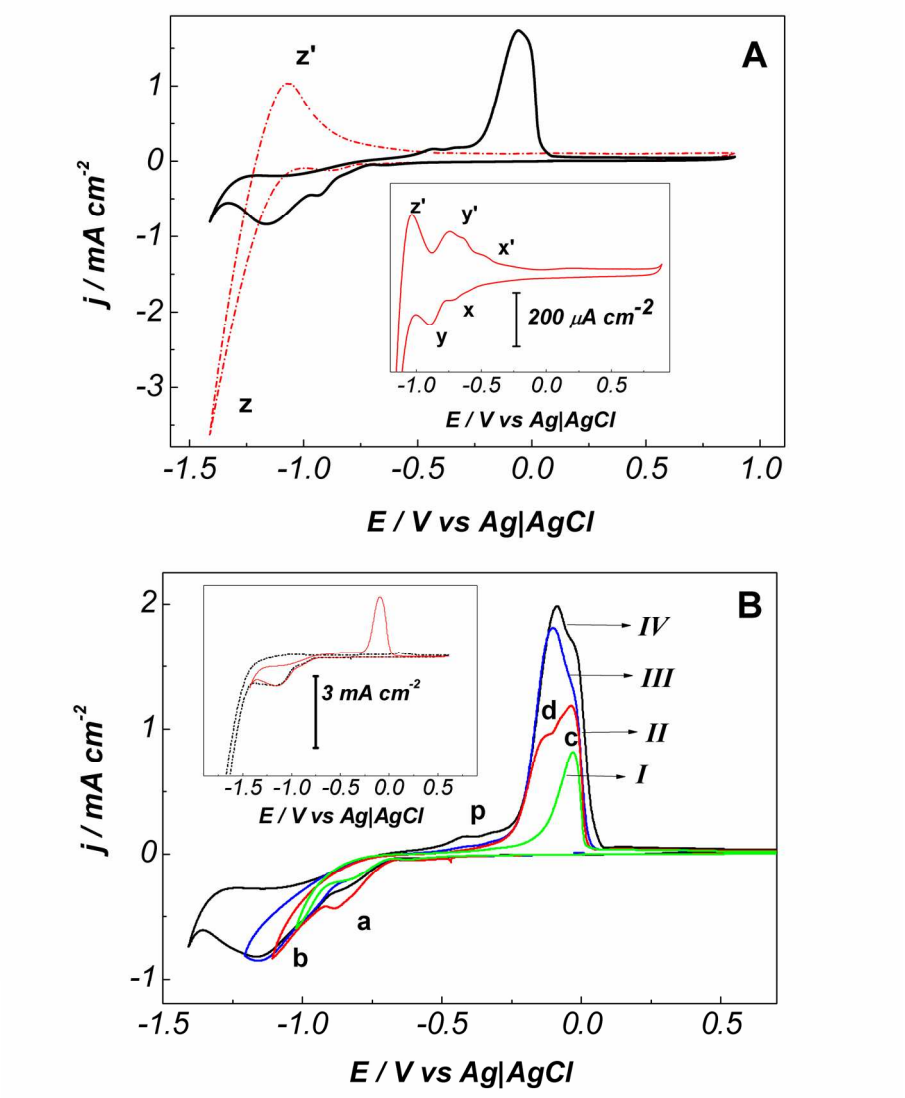

Figure 3

Figure 3

504x624mm (100 x 100 DPI)

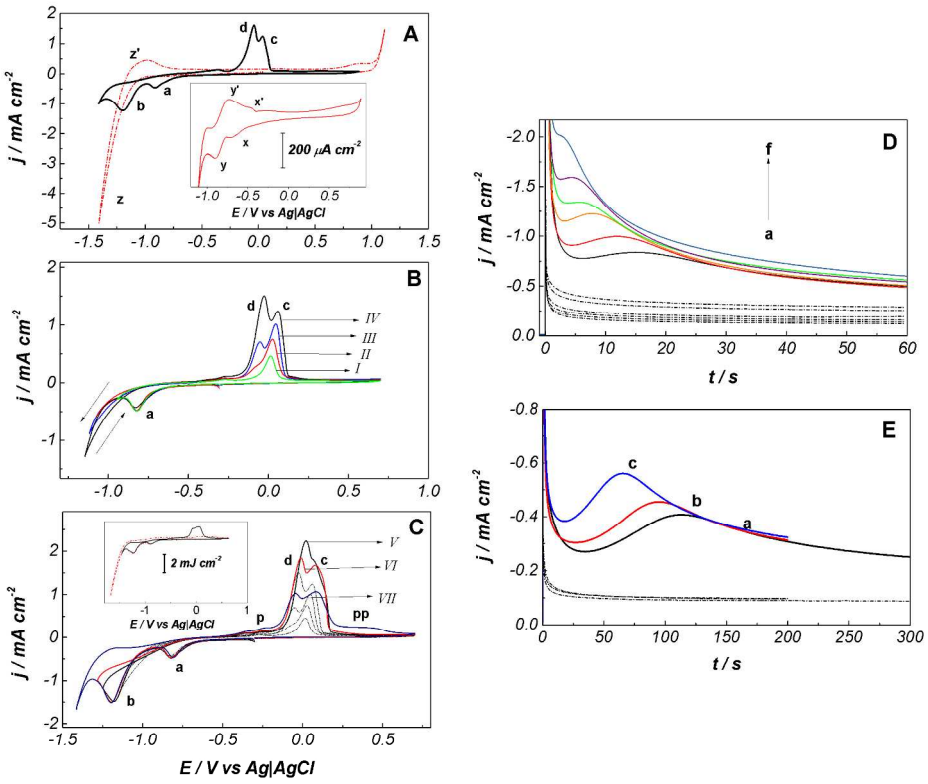

Figure 4

Figure 4

949x800mm (78 x 78 DPI)

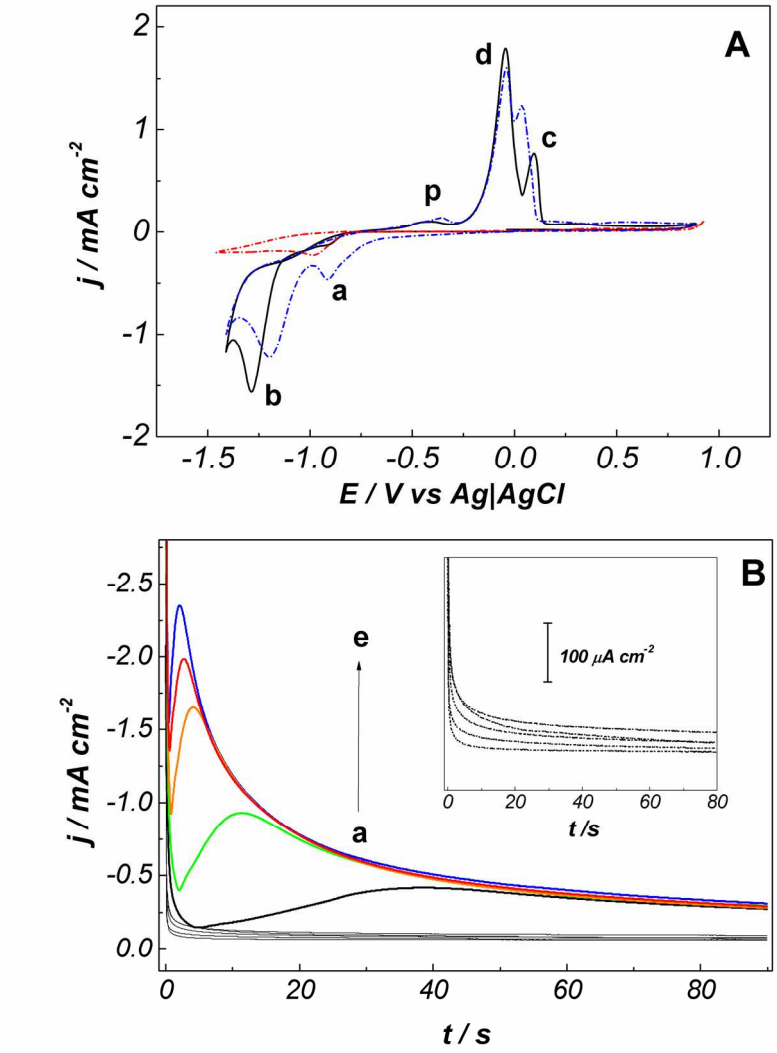

Figure 5

Figure 5

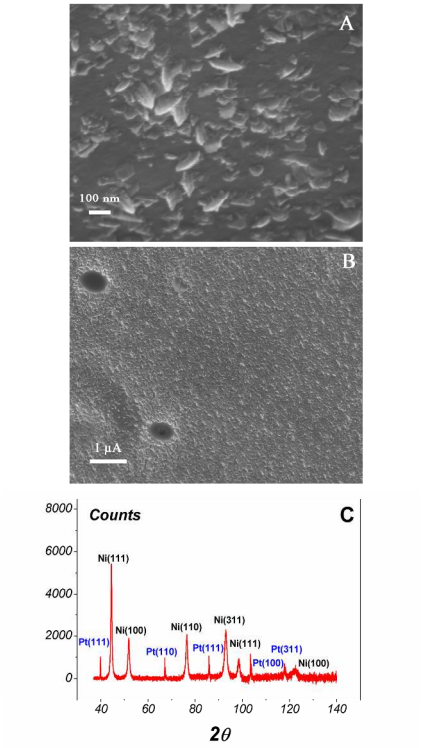

Figure 6

Figure 6

1000x800mm (78 x 78 DPI)

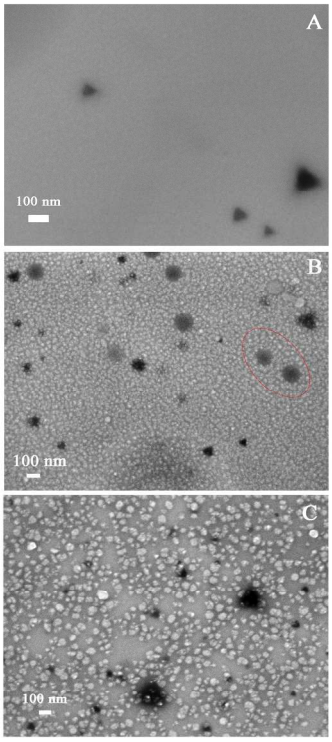

Figure 7

Figure 7

1000x800mm (78 x 78 DPI)

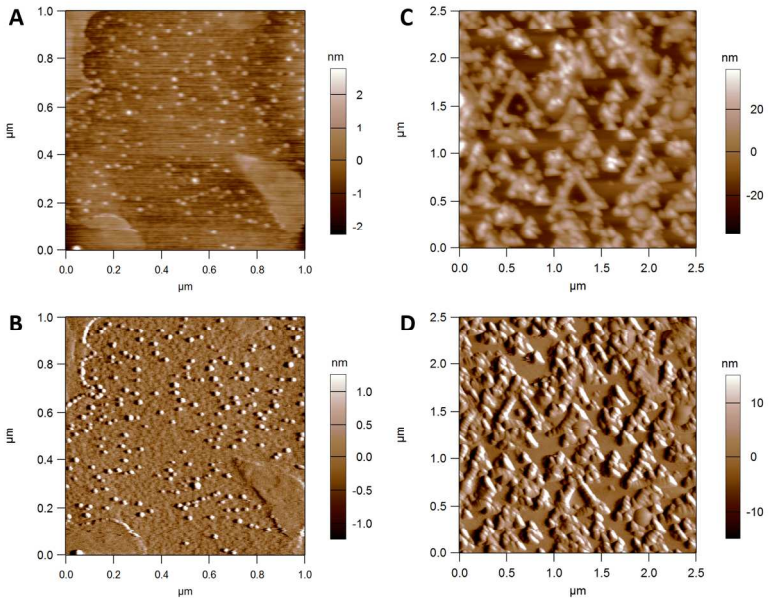

Figure 8

Figure 8

1000x800mm (78 x 78 DPI)

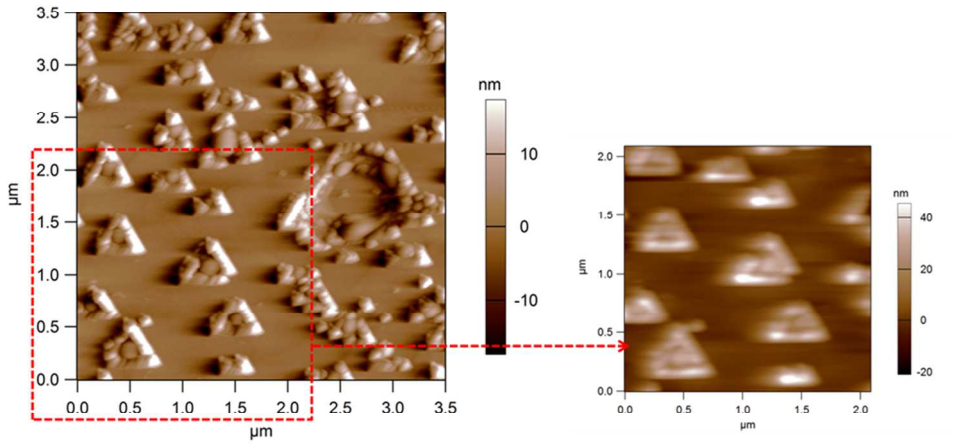

Figure 9

Figure 9

1000x800mm (78 x 78 DPI)